Informes Técnicos Ciemat

1432

Junio, 2018

Water Retention Curves of Bentonite Samples of the Febex Dismantling Project (FEBEX-DP)

G. Campos
Mª. V. Villar

GOBIERNO
DE ESPAÑA

MINISTERIO
DE CIENCIA, INNOVACIÓN
Y UNIVERSIDADES

Ciemat
Centro de Investigaciones
Energéticas, Medioambientales
y Tecnológicas

Informes Técnicos Ciemat

1432
Junio, 2018

Water Retention Curves of Bentonite Samples of the Febex Dismantling Project (FEBEX-DP)

G. Campos
Mª. V. Villar

Departamento de Medio Ambiente

Toda correspondencia en relación con este trabajo debe dirigirse al Servicio de Información y Documentación, Centro de Investigaciones Energéticas, Medioambientales y Tecnológicas, Ciudad Universitaria, 28040-MADRID, ESPAÑA.

Las solicitudes de ejemplares deben dirigirse a este mismo Servicio.

Los descriptores se han seleccionado del Thesauro del DOE para describir las materias que contiene este informe con vistas a su recuperación. La catalogación se ha hecho utilizando el documento DOE/TIC-4602 (Rev. 1) Descriptive Cataloguing On-Line, y la clasificación de acuerdo con el documento DOE/TIC.4584-R7 Subject Categories and Scope publicados por el Office of Scientific and Technical Information del Departamento de Energía de los Estados Unidos.

Catálogo general de publicaciones oficiales
http://www.060.es

Depósito Legal: M-26385-2011
ISSN: 1135-9420
NIPO: 058-18-014-8

Publicación incluida en el programa editorial del suprimido Ministerio de Economía, Industría y Competitividad y editada por el Ministerio de Ciencia, Innovación y Universidades (de acuerdo con la reestructuración ministerial establecida por Real Decreto 355/2018, de 6 de junio

Editorial CIEMAT

CLASIFICACIÓN DOE Y DESCRIPTORES

S58
BENTONITE; TESTING; RADIOACTIVE WASTE STORAGE; HUMIDITY CONTROL;
WATER; RESEARCH PROGRAMS

Water Retention Curves of Bentonite Samples of the Febex Dismantling Project (FEBEX-DP)

Campos, G.; Villar, Mª. V.

44 pp. 30 refs. 42 figs. 7 tables

Abstract:

The FEBEX in situ test simulated the engineered barrier of a nuclear waste repository and was in operation for 18 years under natural conditions. The water retention curves of bentonite samples retrieved during dismantling of the in situ test were determined in wetting paths under isochoric conditions with the vapour transfer technique. The water retention curve relates suction (or relative humidity) to bentonite water content. Samples taken from the drier blocks in the barrier –i.e. those closest to the heater that simulated the waste container– and those from the core of the barrier in cool areas were used, since the aim of the tests was to check the effect of prolonged and intense drying on the water retention capacity of the bentonite.

For the samples tested the initial water content conditioned the retention capacity for suctions above 10 MPa. In contrast, the samples closest to the heater, which had the lowest water contents, reached higher water contents for the lowest suctions than the rest of the samples, which attest that the water adsorption capacity was not lost as a result of prolonged drying.

The comparison of the water retention curves obtained in the retrieved samples with those for the FEBEX reference bentonite compacted at similar densities shows that there were no changes in the water retention capacity during operation and that the water adsorption capacity of the bentonite under constant volume conditions is mostly conditioned by dry density.

FEBEX-DP: Curvas de Retención de la Bentonita

Campos, G.; Villar, Mª. V.

44 pp. 30 refs. 42 figs. 7 tablas

Resumen:

El ensayo in situ FEBEX estuvo en operación durante 18 años simulando a escala real la barrera de ingeniería en un almacenamiento de residuos radiactivos de alta actividad. Se han determinado las curvas de retención de agua de muestras de bentonita tomadas durante el desmantelamiento de dicho ensayo, para lo que se ha utilizado la técnica de transferencia de vapor siguiendo trayectorias de humectación con las muestras mantenidas a volumen constante. La curva de retención relaciona la succión (o humedad relativa) con la humedad de la bentonita. Se han usado muestras tomadas de los bloques más secos que estaban en contacto con el calentador que simulaba el contenedor de residuos y otras muestras de humedad similar tomadas en partes de la barrera no afectadas por el calentador, es decir, frías. El objetivo de estos ensayos ha sido comprobar si el calentamiento intenso y prolongado sufrido por la bentonita en las condiciones de la barrera afecta irreversiblemente la capacidad de retención de la barrera.

Parece que la humedad inicial de las muestras es el factor que más afecta la capacidad de retención de agua para succiones superiores a 10 MPa. Por el contrario, las muestras próximas al calentador, que tenían inicialmente las humedades más bajas, alcanzaron humedades más altas que el resto de las muestras para las succiones más bajas, lo que prueba que la capacidad de adsorción de agua de la bentonita no se perdió como consecuencia del secado prolongado.

La comparación de las curvas de retención obtenidas en las muestras procedentes del ensayo in situ con las de la bentonita FEBEX de referencia compactada a densidades secas similares muestra que no hubo cambios significativos en la capacidad de retención de la bentonita debidos a su uso como material de barrera durante 18 años. La capacidad de retención de la bentonita en condiciones de volumen constante está fundamentalmente condicionada por su densidad seca.

Technical report CIEMAT/DMA/2G218/4/18

WATER RETENTION CURVES OF BENTONITE SAMPLES OF THE FEBEX DISMANTLING PROJECT (FEBEX-DP)

AUTHORS: Gemma **Campos,** María Victoria **Villar**

May 2018

WATER RETENTION CURVES OF BENTONITE SAMPLES OF THE FEBEX DISMANTLING PROJECT (FEBEX-DP)

Table of contents

TABLE OF CONTENTS I

1. INTRODUCTION 1

2. DISMANTLING OF THE BARRIER AND BENTONITE SAMPLING 4

3. THE FEBEX BENTONITE 9

4. METHODOLOGY 10

4.1. SUCTION MEASUREMENT 11
4.2. WATER CONTENT AND DRY DENSITY 12
4.3. MEASUREMENT OF BASAL SPACING 12
4.4. PORE SIZE DISTRIBUTION 13
4.5. WATER RETENTION CURVES 13

5. RESULTS 15

5.1. COMPUTATION OF DEGREE OF SATURATION 15
5.2. BASIC PROPERTIES 16
5.3. WATER RETENTION CURVE 18
5.4. PORE SIZE DISTRIBUTION OF TESTED SAMPLES 27
5.5. INTERLAYER SPACE OF TESTED SAMPLES 31

6. DISCUSSION 33

7. SUMMARY AND CONCLUSIONS 38

7.1. THE FEBEX IN SITU TEST 38
7.2. WATER RETENTION CURVES DETERMINATION 39
7.3. WATER RETENTION CURVE RESULTS 40
7.4. CLOSURE 41

ACKNOWLEDGEMENTS 41

LIST OF REFERENCES 42

1. Introduction

The aim of FEBEX (Full-scale Engineered Barriers Experiment) was to study the behaviour of components in the near-field for a high-level radioactive waste (HLW) repository in crystalline rock. The project was based on the Spanish reference concept for disposal of radioactive waste in crystalline rock (AGP Granito): the waste canisters are placed horizontally in drifts and surrounded by a clay barrier constructed from highly-compacted bentonite blocks (ENRESA 1995). As part of this project, an "in situ" test, under natural conditions and at full scale, was performed at the Grimsel Test Site (GTS, Switzerland), an underground laboratory managed by NAGRA (the Swiss agency for nuclear waste management). The thermal effect of the wastes was simulated by means of heaters, whereas hydration was natural (ENRESA 2000, 2006).

The basic components of the test (Fig. 1) were: the gallery, measuring 70 m in length and 2.3 m in diameter, excavated through the Aare granite; the heating system, made up of two heaters placed inside a liner installed concentrically with the gallery and separated one from the other by a distance of 1.0 m, with dimensions and weights analogous to those of the real canisters; the clay barrier, formed by blocks of compacted bentonite; the instrumentation and the monitoring and control system for data acquisition and supervision and control of the test. Up to 632 sensors of very diverse types were initially installed to monitor the different thermo-hydro-mechanical processes that occurred in both the clay barrier and the surrounding rock throughout the entire life of the test. The gallery was closed by a concrete plug.

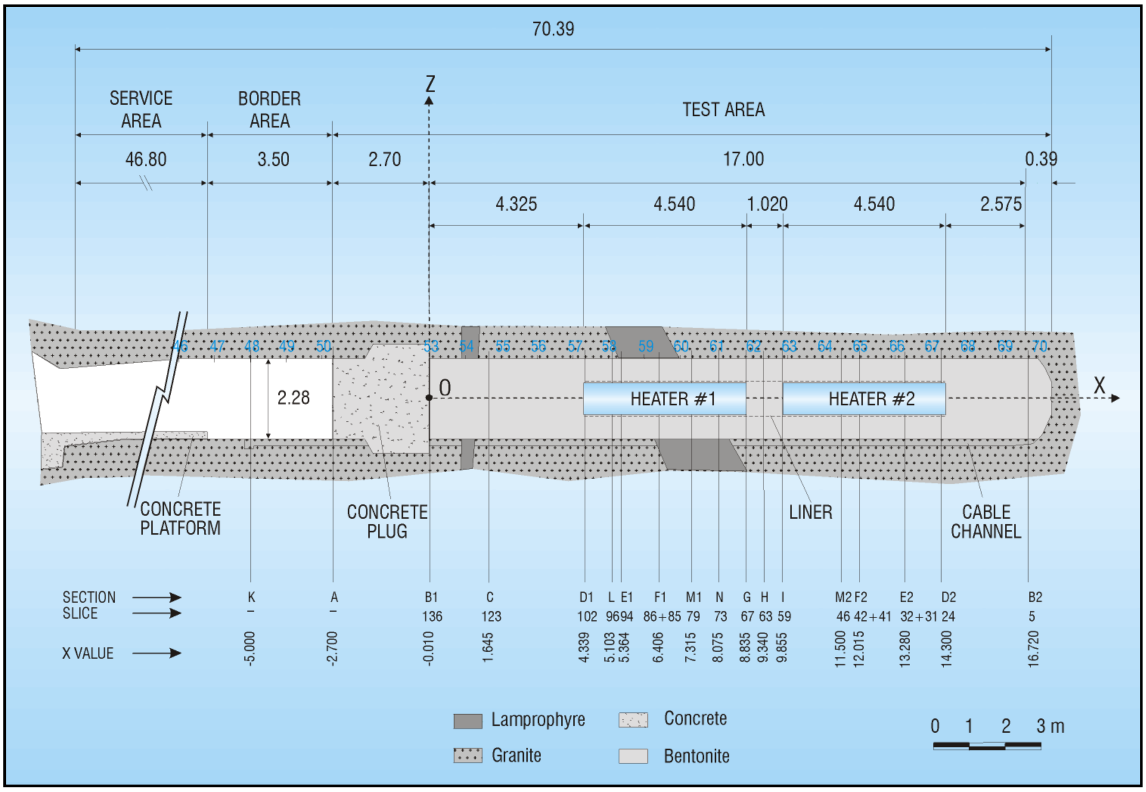

Fig. 1: General layout of the in situ test during phase I, including instrumented sections (ENRESA, 2000)

The clay barrier was made of FEBEX bentonite, which was extracted from the Cortijo de Archidona deposit (Almería, Spain) and whose main characteristics are summarised in Chapter

3. To build the clay barrier, various types of blocks were manufactured from the bentonite in the shape of 12-cm thick circular crown sectors. The blocks were arranged in vertical slices consisting of concentric rings. In the heater areas the interior ring was in contact with the steel liner, whereas in the non-heater areas a core of bentonite blocks replaced the heaters (Fig. 2). The geometry of the blocks is shown in Fig. 2. The thickness of the bentonite barrier in the heater areas was 65 cm (distance from liner to granite). The backfilled area was sealed with a plain concrete plug placed into a recess excavated in the rock.

The blocks were obtained by uniaxial compaction of the FEBEX clay with its hygroscopic water content at pressures of between 40 and 45 MPa, what caused dry densities of 1.69-1.70 g/cm^3. The initial dry density of the blocks was selected by taking into account the probable volume of the construction gaps and the need to have a barrier with an average dry density of 1.60 g/cm^3 (ENRESA, 2000).

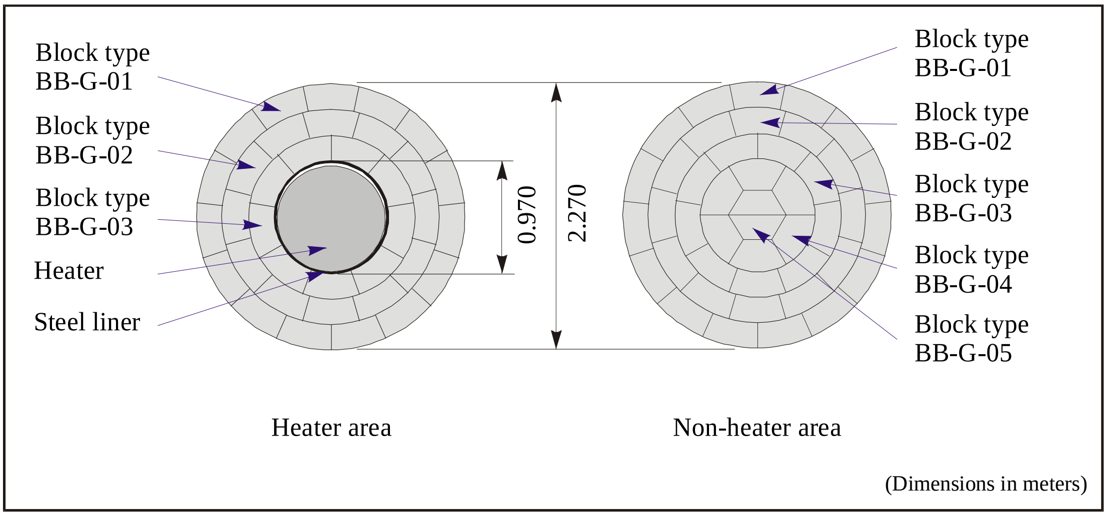

Fig. 2: Geometry of the clay barrier in the FEBEX *in situ* test at GTS (ENRESA 2000)

The heating stage of the in situ test began on February 27th 1997. The power of the heaters was adjusted so that to keep the temperatures at the liner surface at 100ºC. After five years of uninterrupted heating at constant temperature, the heater closer to the gallery entrance (Heater #1) was switched off (February 2002). In the following months this heater and all the bentonite and instruments preceding and surrounding it were extracted (Bárcena et al., 2003). A large number of bentonite samples were taken for analysis in different laboratories (Villar et al. 2006). The remaining part of the experiment was sealed with a new sprayed shotcrete plug. New sensors were installed in the buffer through the shotcrete plug, and a second operational phase started with the test configuration shown in Fig. 3. The buffer and all components were removed up to a distance of 2 metres from Heater #2 to minimize disturbance of the non-dismantled area. A dummy steel cylinder with a length of 1 m was inserted in the void left by Heater #1 in the centre of the buffer.

The test continued running until April 2015, when Heater #2 was switched off and the dismantling operations started. Many sensors were in operation until the end of the experiment, which allowed to follow the evolution of some thermo-hydro-mechanical variables during the second operational phase (Martínez et al. 2016). The relationship between the temperatures measured before dismantling and the distance from the gallery axis in vertical sections is represented in Fig. 4. Each curve shows the measuring results in the same vertical instrumented section, whose locations are indicated in Fig. 3. The same results are plotted in Fig. 5 along a longitudinal section of the gallery.

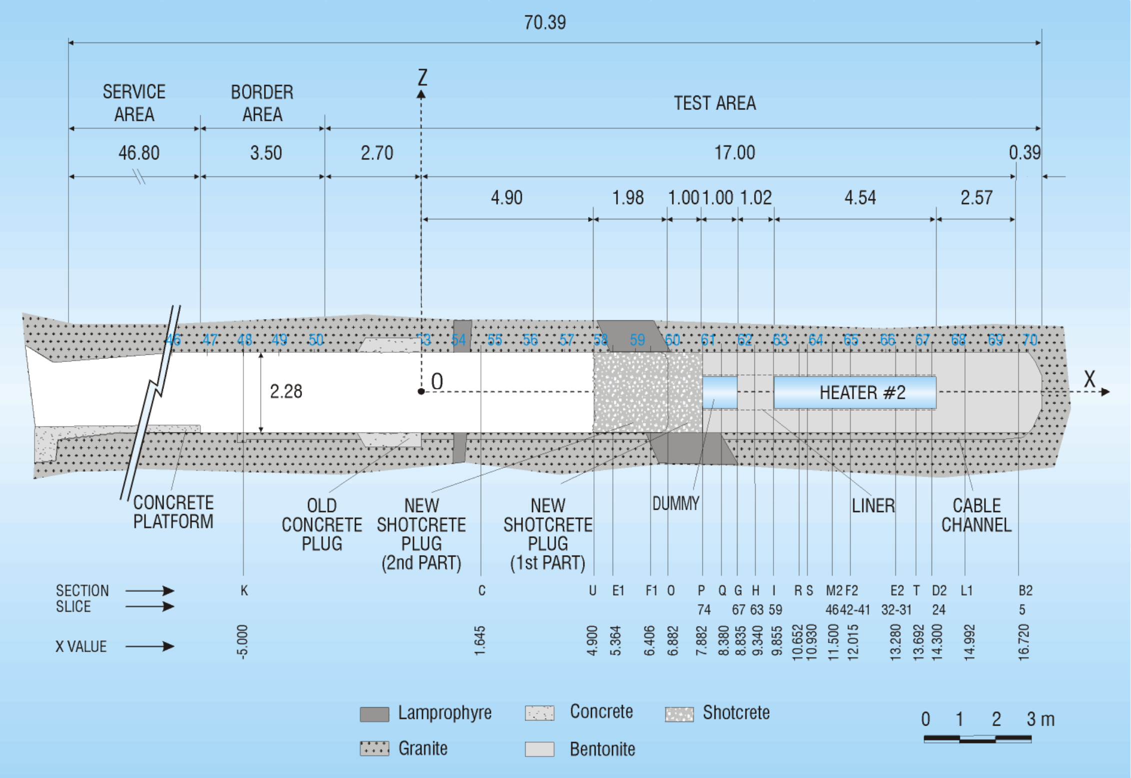

Fig. 3: General layout of the in situ test during phase II, including instrumented sections (ENRESA 2006)

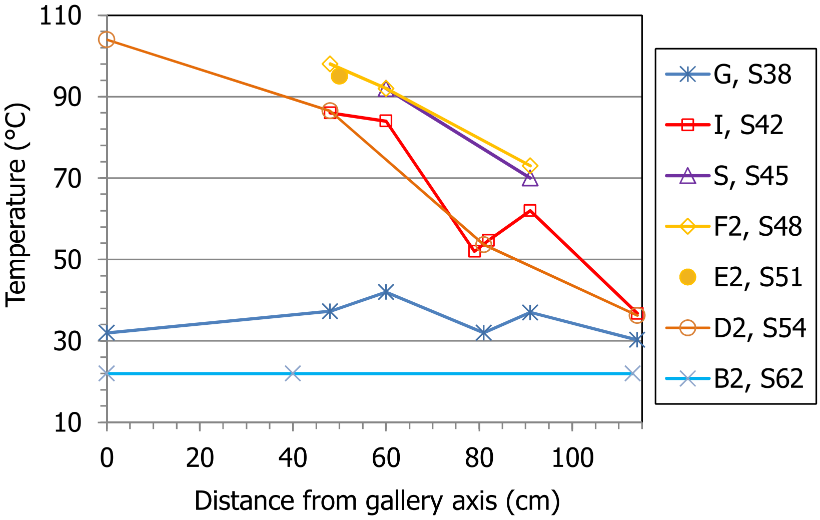

Fig. 4: Steady temperatures measured during operation by thermocouples located in different instrumented sections (Villar et al. 2018a). See Fig. 3 for location of instrumented sections, the correspondence with the sampling sections shown in Fig. 9 is indicated in the legend

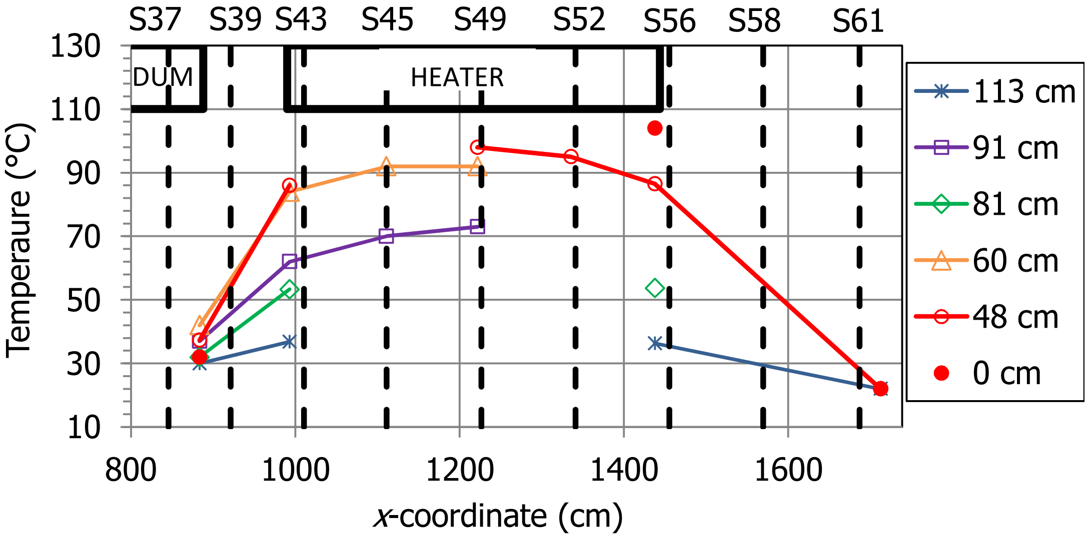

Fig. 5: Steady temperatures along the gallery axis measured during operation by thermocouples located in different instrumented sections. The distance of the sensors to the gallery axis is indicated in the legend. The position of some sampling sections along the gallery is indicated by thick dotted vertical lines (Villar et al. 2018a)

The dismantling operations included the demolition of the shotcrete plug and the removal of all the bentonite in front of, surrounding the heater and at the back of it. A large number of samples from all types of materials were taken for analysis. In particular, clay samples were taken to characterise the solid and liquid phases, in order to confirm predictions and validate existing models of THM and THG processes.

This document collects the results obtained by CIEMAT referring to part of the hydraulic characterisation of the samples, namely the determination of their water retention curves (WRC). The whole thermo-hydro-mechanical (THM) characterisation of the samples (including a summary of the results presented here) was presented in Villar et al. (2018b). For completeness, some of the results presented in that report are presented here again, because they have been used to complement and interpret the WRC results. The results of the bentonite characterisation obtained by all the project partners were also summarised in the synthesis report NAB-16-017 (Villar 2017).

2. Dismantling of the barrier and bentonite sampling

The test continued running until April the 24th 2015, when Heater #2 was switched off. The shotcrete plug started to be demolished some days earlier, and the buffer removal and sampling took place between May 8th and August 5th, as the temperature in the area affected by the dismantling should be reduced to a level compatible with manual works (25-30°C). This means that when the first bentonite section was sampled, the heater had been switched-off for 14 days, and as sampling proceeded, the more towards the back of the gallery the sampling section was, the longer its cooling period had been. All details about the sampling program are given in NAB15-014 (Bárcena & García-Siñeriz 2015).

The on-site determinations performed during dismantling showed that the physical conditions of the bentonite along the barrier had changed during operation, as a result of hydration and of the different temperatures to which the bentonite had been subjected (Fig. 4, Fig. 5). Water content and dry density gradients, both across the vertical sections and along the gallery, had been generated (Villar et al. 2016). Fig. 6 to Fig. 8 show the final distribution of dry density, water content and degree of saturation along the barrier obtained from the on-site determinations. It is clear that the conditions of the samples taken depended on the exact location along the barrier of the sampling section from which they were taken, as well as on the position of a particular sample with respect to the axis of the gallery. The main differences occurred between the sections located around the heater (sections S42 to S53) and those in cool areas.

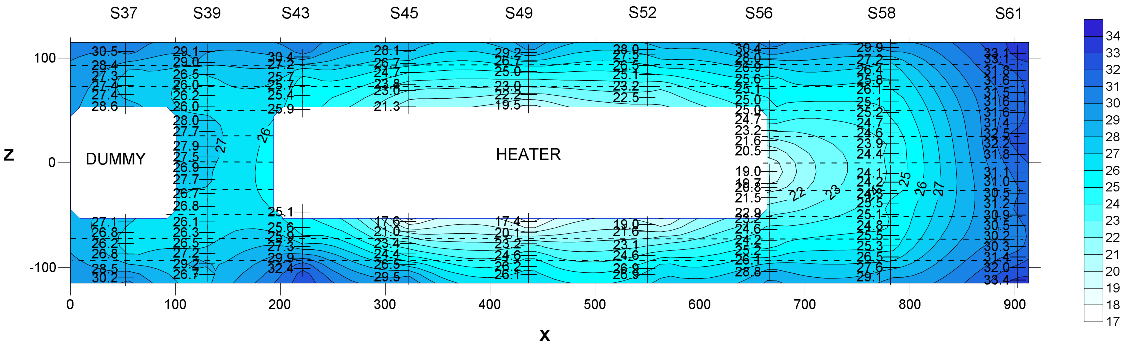

Fig. 6: Water content distribution in a vertical longitudinal section (Villar et al. 2016)

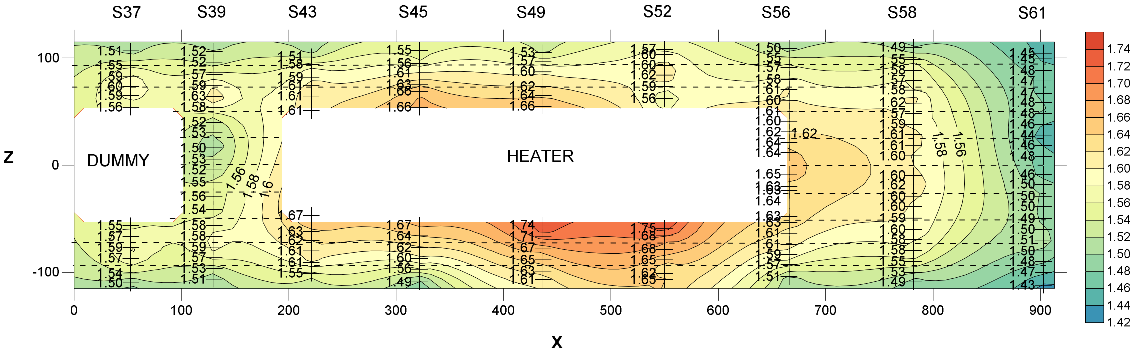

Fig. 7: Dry density distribution in a vertical longitudinal section (Villar et al. 2016)

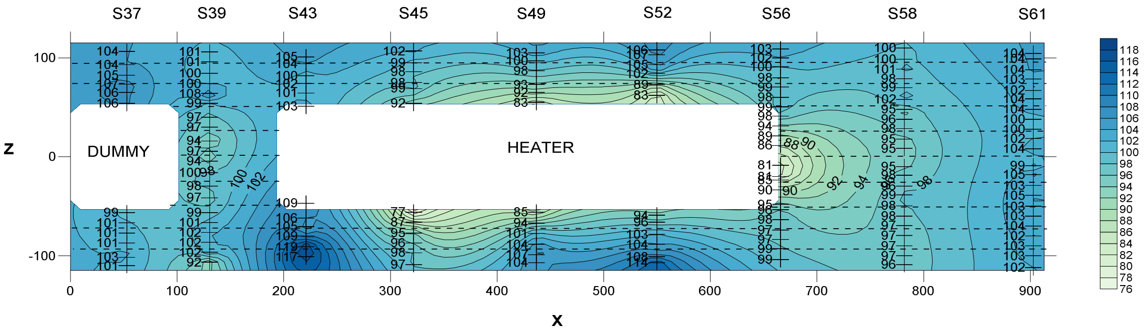

Fig. 8: Degree of saturation distribution in a vertical longitudinal section (Villar et al. 2016) (inexact values because of solid specific weight and water density uncertainties)

The location of the bentonite sampling points was fixed to allow a good representation of physico-chemical alterations and hydration distribution. The sampling took place in vertical sections normal to the axis of the tunnel, and in each section several samples were taken along different radii. The sections were numbered from the entrance of the gallery towards the back of it, and the numbering started in the first dismantling. Hence, sampling sections S31 to S61 were sampled in 2015.

The bentonite samples sent to CIEMAT and used for their thermo-hydro-mechanical (THM) and thermo-hydro-geochemical (THG) characterisation were taken from the vertical sections detailed in Fig. 9. The exact location of the block samples inside each section is shown in Fig. 10. The blocks were preserved in plastic film, two layers of aluminised PET-sheets and vacuum-sealed plastic bags immediately after their extraction. The PET-sheets were vacuum-sealed. Protection against mechanical actions was used to ensure the integrity of the material. The samples were referred to according to the key given in the Sampling Book (Bárcena & García-Siñeriz 2015). A summary of the results obtained by CIEMAT on the basic and thermo-hydro-mechanical characterisation of the bentonite retrieved during the dismantling was presented in Villar et al. (2018b). The laboratory sampling logs of the samples analysed at CIEMAT are compiled in Iglesias et al. (2018). The mineralogical and geochemical characteristics of the same blocks are presented in Fernández et al. (2018). Other laboratories also received bentonite samples and the results obtained by all of them –including CIEMAT– on bentonite characterisation were summarised and analysed in Villar (2017).

Tab. 1 shows the blocks from which the samples for the water retention curve determination were obtained and the radius of the section along which they were taken, according to Fig. 11. The radii were named according to the same key used for the on-site determinations (Villar et al. 2016). The date of the block retrieving at Grimsel (Retrieving GTS), of its arrival at CIEMAT (Arrival CIEMAT) and of its sampling at CIEMAT's laboratories (Sampling CIEMAT) are indicated in the Table, along with the time elapsed from the day they were taken until they were sampled in the laboratory. This time span was quite broad, between 84 and 189 days, mainly because it took three months for the first samples to get to CIEMAT. Most of the samples were received on August 7th and 21st. The Table also indicates if the samples were still vacuum sealed when they were sampled at CIEMAT or not.

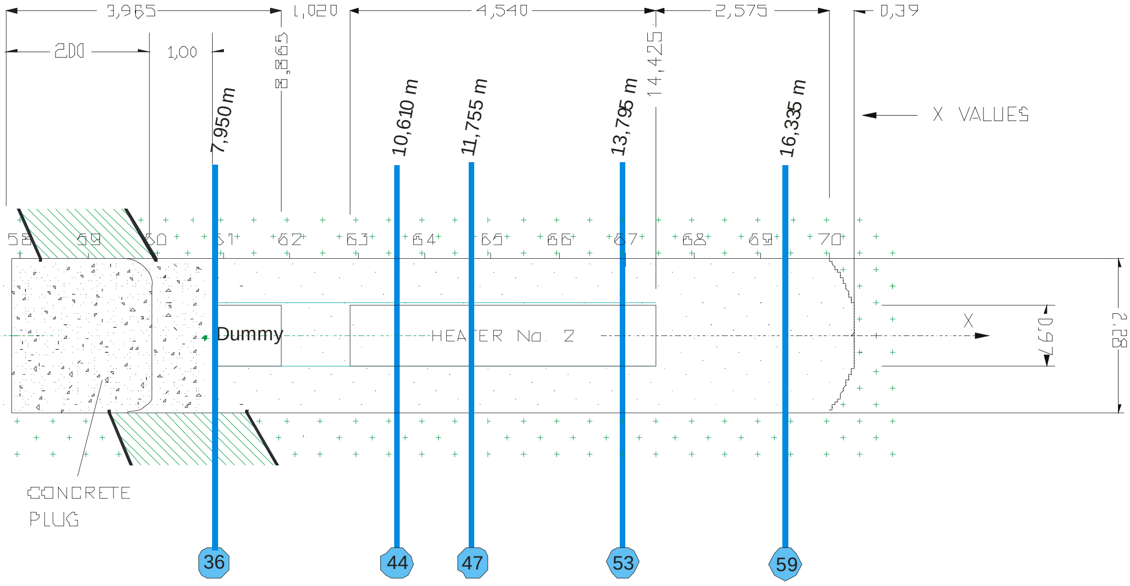

Fig. 9: Distribution of sampling sections for THM-THG studies at CIEMAT (modified from Bárcena & García-Siñeriz 2015)

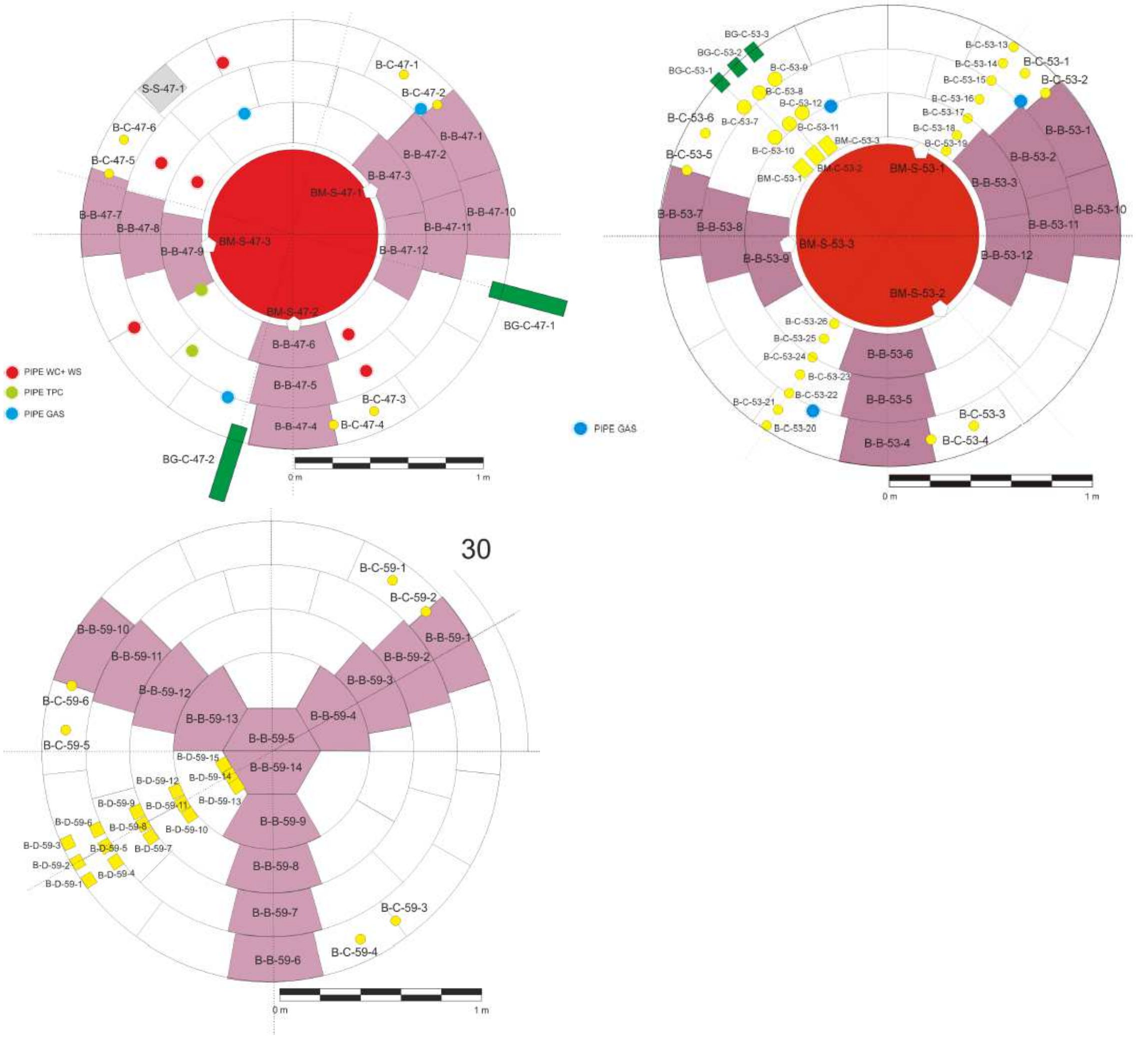

Fig. 10: Position of blocks received at CIEMAT for THM and THG tests in sampling sections S47, S53 and S59 (Bárcena & García-Siñeriz 2015)

Tab. 1: Summary of blocks sampled at CIEMAT for water retention curve determination

Section	**Radius**	**Block reference**	**Retrieving GTS**	**Arrival CIEMAT**	**Sampling CIEMAT**	**Time elapsed (days)**	**Vacuum**
S47	B	BB-47-3	26/6/15	7/8/15	9/9/15	75	yes
S47	D	BB-47-6	29/6/15	7/8/15	26/10/15	119	no
S47	E-F	BB-47-9	29/6/15	7/8/15	19/10/15	112	yes
S53	B	BB-53-3	15/7/15	21/8/15	13/1/16	182	no
S53	D	BB-53-6	15/7/15	21/8/15	19/1/16	188	no
S53	E-F	BB-53-9	15/7/15	21/8/15	20/1/16	189	yes
S59	B	BB-59-5	28/7/15	21/8/15	16/11/15	111	yes
S59	D	BB-59-14	29/7/15	21/8/15	16/12/15	140	yes

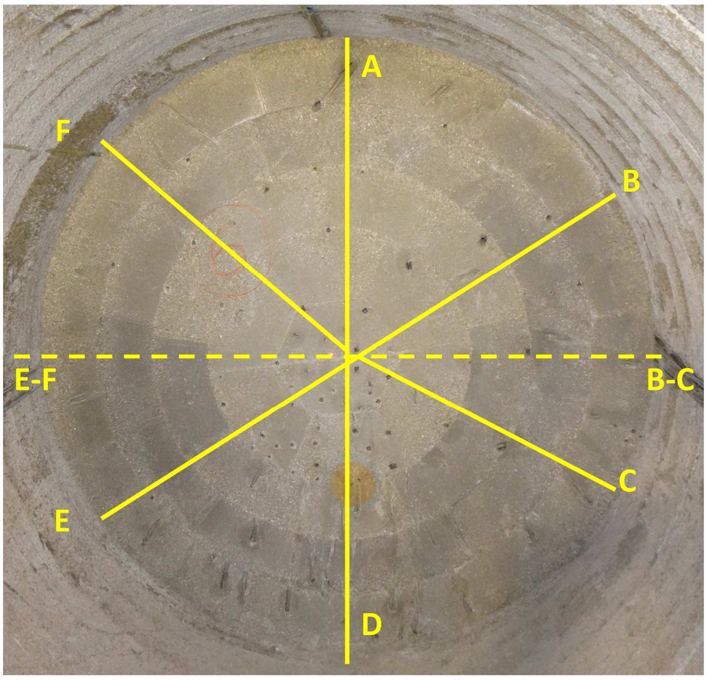

Fig. 11: References for the radii along which the blocks were taken

From their arrival the samples were kept in a RH-controlled room (Fig. 12). The RH was initially set to 70% and then to 80%, although because the samples were vacuum sealed, this value is not considered relevant. In fact, from February 2016 on, the RH control stopped working. The evolution of temperature and RH in this room for the period in which the FEBEX-DP samples were stored in it for analysis is shown in Fig. 13.

Fig. 12: RH-controlled room for the storage of samples

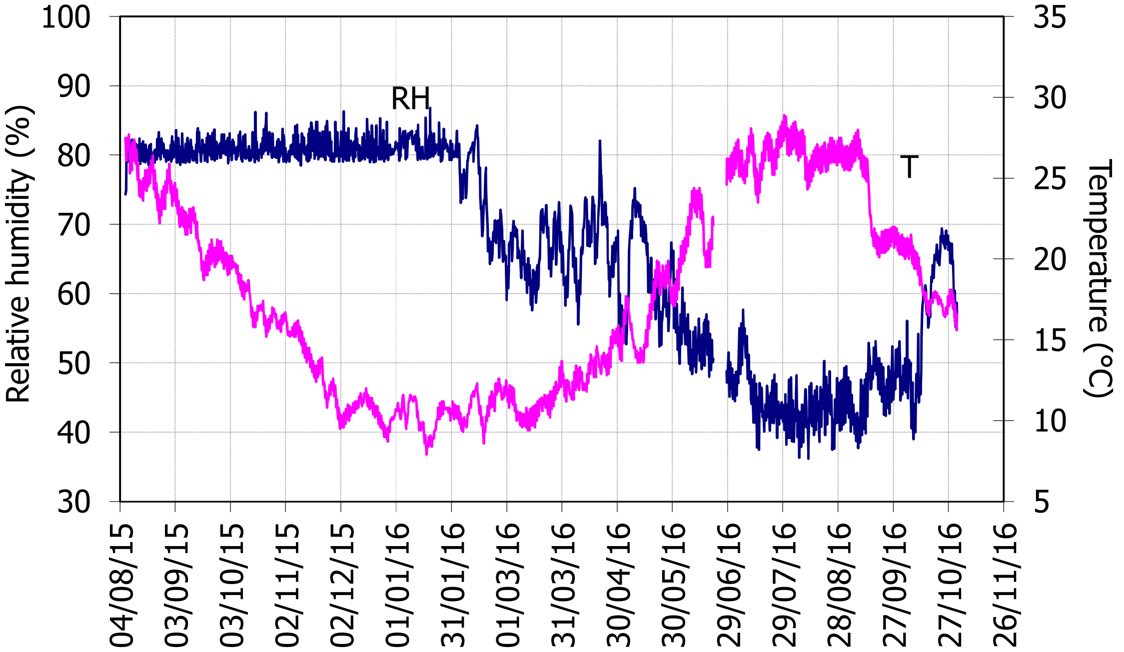

Fig. 13: Relative humidity and temperature in the storage room over the sampling and testing period

3. The FEBEX bentonite

The FEBEX bentonite was extracted from the Cortijo de Archidona deposit (Almería, Spain) and the processing at the factory consisted on disaggregation and gently grinding, drying at 60°C and sieving by 5 mm. The physico-chemical properties of the FEBEX bentonite, as well as its most relevant thermo-hydro-mechanical and geochemical characteristics obtained during the projects FEBEX I and II were summarised in the final reports of the projects (ENRESA, 2000, 2006), and later documents (Villar & Gómez-Espina 2009). A summary of the results obtained relevant for this report is given below.

The montmorillonite content of the FEBEX bentonite is above 90 wt.% (92±3 %). The smectitic phases are actually made up of a smectite-illite mixed layer, with 10-15 wt.% of illite layers. Besides, the bentonite contains variable quantities of quartz (2±1 wt.%), plagioclase (3±1 wt.%), K-felspar (traces), calcite (1±1 wt.%), and cristobalite-trydimite (2±1 wt.%).

The cation exchange capacity of the smectite is 102±4 meq/100g, the main exchangeable cations being calcium (35±2 meq/100g), magnesium (31±3 meq/100g) and sodium (27±1 meq/100g). The predominant soluble ions are chloride, sulphate, bicarbonate and sodium.

The liquid limit of the bentonite is 102±4 %, the plastic limit 53±3 %, the density of the solid particles 2.70±0.04 g/cm^3, and 67±3 % of particles are smaller than 2 µm. The hygroscopic water content in equilibrium with the laboratory atmosphere (relative humidity 50±10 %, temperature 21±3 °C, total suction about 100 MPa) is 13.7±1.3 %. The external specific surface area is 32±3 m^2/g and the total specific surface area is about 725 m^2/g.

The saturated hydraulic conductivity of compacted bentonite samples is exponentially related to their dry density. For a dry density of 1.6 g/cm^3 the saturated permeability of the bentonite is approximately $5 \cdot 10^{-14}$ m/s at room temperature, either with diluted granitic or deionised water used as percolating fluid. The temperature increase tends to increase permeability.

The swelling pressure of compacted samples is also exponentially related to the bentonite dry density. The bentonite compacted at dry density of 1.6 g/cm^3 and saturated with deionised water at room temperature develops a swelling pressure of about 6 MPa. Saturation with a Spanish diluted granitic water gives similar values, whereas temperature causes a decrease of them.

The retention curve of the bentonite was determined in samples compacted to different dry densities at different temperatures (Lloret *et al*. 2004, Villar & Lloret 2004, Villar & Gómez-Espina 2009). The volume of the samples remained constant during the determinations, since they were confined in constant volume cells. Following an approach similar to that presented by Sánchez (2004) to fit the data from these laboratory determinations, the empirical Equation 1 was obtained:

$$w = \left(b \cdot n^{c} \cdot e^{-\alpha\cdot(T-T_0)}\right) \cdot \left[1 + \left(\frac{s}{P_0 \cdot e^{-\eta\cdot(n-n_0)} \cdot e^{-\alpha\cdot(T-T_0)}}\right)^{\frac{1}{1-\lambda_1}}\right]^{-\lambda_1} \cdot \left(1 - \left(\frac{s}{P_{sec}}\right)^{\lambda_2}\right) \cdot (S_r - S_{lr})$$

[1]

where w is the water content (%), n and n_0 are the porosity and reference porosity, respectively, s is the suction (MPa), T and T_0 are the temperature and reference temperature, respectively, (ºC), S_r and S_{lr} are the liquid degree of saturation and liquid residual degree of saturation, respectively, P_0, P_{sec}, λ_1 and λ_2 are the parameters to define the shape of the retention curve at the reference temperature and porosity, and b, c, α and η are fitting parameters that take into account the influence of temperature and porosity. The values of parameters are indicated in Tab. 2. The differences between measured values and the estimated values using Equation 1 are smaller than 2% in terms of water content.

Tab. 2: Values of parameters in Equation 1

b	c	P_0 (MPa)	λ_1	λ_2	η	n_0	α (1/ºC)	T_0 (ºC)	P_{sec} (MPa)	S_r	S_{lr}
145	1.9	25	0.2	1.1	20	0.4	0.0015	20	1000	1.0	0.01

4. Methodology

The laboratory determinations presented in this report were carried out at CIEMAT facilities mostly from August 2015 to December 2017. During the main testing period, between one and three blocks were sampled every week in the laboratory. The block to be sampled every day was taken early in the morning from the storage room to the laboratory where the subsampling was made. Some blocks were taken out from the storage room a day before sampling, since thermal equilibrium is necessary for the correct measurement of thermal conductivity and suction.

The plastic and aluminium foil bags were removed and, with the block wrapped in the plastic foil, thermal conductivity and relative humidity were measured. To perform these measurements only the indispensable surface of the block was uncovered, so that to avoid unnecessary humidity losses.

Each block was unpacked only once in order to take the subsamples for the different determinations. The sampling was coordinated to make the tests immediately after unpacking and sampling. The blocks were sectioned along the radius, in order to obtain material for the hydro-mechanical (THM) and geochemical and mineralogical (THG) tests (Fig. 14 left). In order to obtain a more detailed sampling, subsamples from two (three in a few cases) different positions along the radius of the block were taken. The subsamples obtained in this way were referenced by adding a correlative number to the initial reference of the block, 1 for the closest part to the granite and 2 for the closest part to the gallery axis. The samples for the different HM determinations were obtained by drilling (Fig. 14 right). The sampling logs of the blocks analysed for THM and THG tests are presented in Iglesias et al. (2018).

In the following subchapters the methodology followed for some of the determinations performed is described. Although this report focuses on the water retention curves and the rest of THM determinations were spread out in Villar et al. (2018b), the methodology followed for some of the analysis that have been used to complement or interpret the WRCs is included here again for completeness, as well as some of the results.

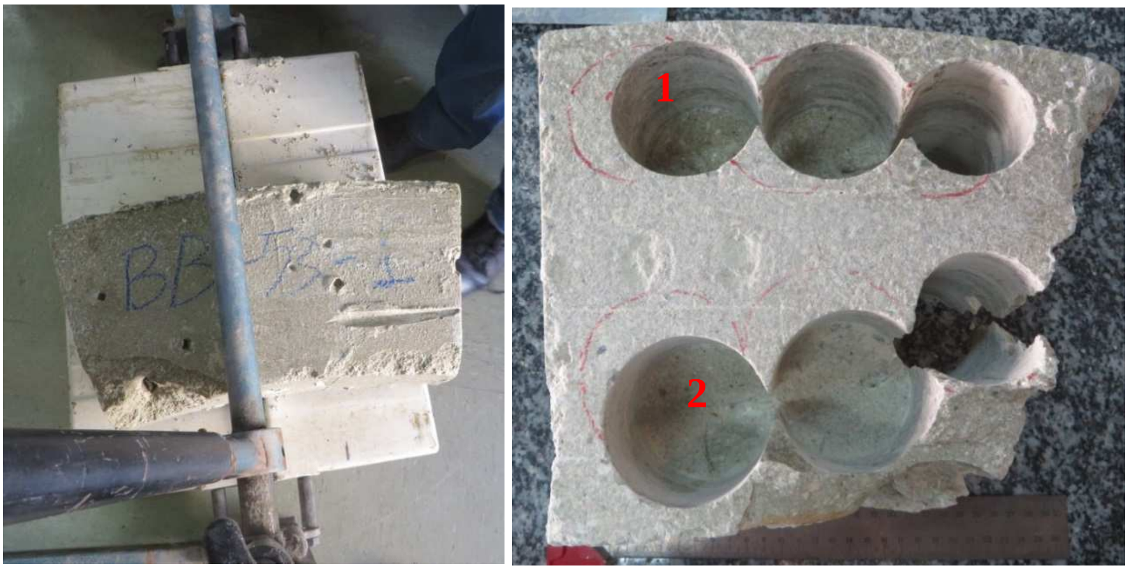

Fig. 14: Sectioning of blocks for THM and THG determinations (left) and drilling of a block to obtain subsamples 1 (closest to the granite) and 2 (closest to the gallery axis) for the HM determinations (right)

4.1. Suction measurement

The relative humidity and temperature of the blocks was measured before unpacking either with psychrometers or with capacitive sensors, depending on the bentonite water content. The relative humidity of the blocks with higher water content was measured with psychrometers. The capacitive transmitters used for the samples with lower water content –which is the case of all the samples used for WRC determinations– were Sensirion SHT75, which have a precision of 2% RH in the range from 20 to 80%.

The blocks were taken to the laboratory at least 1 h before the measurements. The plastic and aluminium foil bags were removed and, with the block wrapped in plastic foil, holes were drilled in the block to install the sensors inside (Fig. 15). The stabilisation of the measurement took about 1 h. To convert the values of relative humidity (RH, %) to suction values (s, MPa) the Kelvin's law is used:

$$s = -10^{-6}\,\frac{R \times T}{V_{\mathrm{w}}}\ln\left(\frac{\mathrm{RH}}{100}\right) \qquad [2]$$

where R is the universal constant of gases (8.3143 J/mol·K), T the absolute temperature and V_{w}, the molar volume of water ($1.80 \cdot 10^{-5}$ m^3/mol).

Fig. 15: Psychrometers inserted into a block prior to unpacking

4.2. Water content and dry density

The samples for the water content and dry density determinations were obtained by drilling with a crown drill bit of internal diameter 4.5 cm. Two or three positions were drilled in each block, and from every core 1 or 2 subsamples were obtained. In each of these subsamples water content and dry density were determined.

The gravimetric water content (*w*) is defined as the ratio between the mass of water and the mass of dry solid expressed as a percentage. Consequently, all the values given in this report are weight percentages. The mass of water was determined as the difference between the mass of the sample and its mass after oven drying at 110°C for 48 h (mass of dry solid). Dry density (ρ_d) is defined as the ratio between the mass of the dry sample and the volume occupied by it prior to drying. The volume of the specimens was determined by immersing them in a recipient containing mercury and by weighing the mercury displaced, taking a fixed density of mercury of 13.6 g/cm^3. The absolute error of this measurement is in the order of 10^{-2} g/cm^3. The same samples whose volumes had been determined were used for the water content determination. The balance used was an AND GF2000, with a capacity up to 2100 g and a precision of 0.01 g.

4.3. Measurement of basal spacing

The (001) reflection or basal spacing gives the distance along the crystallographic c-axis between clay lamellae, and for a given clay depends on the exchangeable cations present in the interlayer and their degree of hydration.

From all the blocks sampled at CIEMAT, subsamples were preserved in paraffined foil and the X-ray profile of a plane surface of them was registered at laboratory temperature after removing the foil and without any further treatment. An anticathode of Cu (CuKα) radiation was used with a Philips model X'Pert-MPD diffractometer at 40 mA, 45 kV operating condition. X-ray diffraction (XRD) experimental profiles were obtained with a 0.1 mm entrance slit and a scanning rate of 0.025 °2θ/s. Data were collected between 2 and 10°2θ. The goniometer settings were: automatic divergence slit and diffracted beam slit 2 mm. The position of the peaks was adjusted by using the quartz in the samples as an internal standard. The complete mathematical description of the scan pattern was obtained by combination of a polynomial function that describes the background and a profile function that fits the experimental peaks in order to obtain better peak parameters (peak position, net intensity and full width at half maximum (FWHM)). The pseudo-Voigt profile function, which is the weighted mean between a Lorentz and a Gaussian function, was used to fit the peaks as well as to deconvolute overlapped peaks.

After the determination of the water retention curves, a fragment of the samples tested was also used for measuring the basal spacing. For these samples an anticathode of Cu (CuKα) radiation was used with a Bruker D8 Advance diffractometer at 40 mA and 40 kV operating conditions. XRD experimental profiles were obtained with a 1 mm entrance slit, 0.05º 2θ step size and a counting time of 3 s per step. Data were collected between 2 and 30° 2. Goniometer settings were fixed divergence slit and diffracted beam slit, both of 1 mm. A profile function was fitted to the observed intensities in order to obtain better peak parameters (peak position, net intensity and full width at half maximum (FWHM)) completely describing the measured scan. The Pearson VII function was used. It was also used to deconvolute overlapped peaks.

4.4. Pore size distribution

The pore size distribution of subsamples from the blocks was determined by mercury intrusion porosimetry (MIP). This technique allows the determination of the pore size distribution by injecting mercury into the sample at different pressures while controlling the volume intruded. The pressure applied can be related to the minimum pore diameter intruded, taking into account the characteristics of the fluid. The ratio of the volume of mercury intruded (pore volume) to the applied pressure (which conditions the minimum pore diameter) allows distribution curves to be obtained establishing the percentage of pores of a size included within a given range.

In order to alter as less as possible the clay microstructure during drying, the samples were put in the ice condenser of a Telstar LioQuest equipment at -50°C for 3 h. Afterwards they were lyophilised for 19 h at a temperature of -50°C under a vacuum of 0.2 mbar, so that to eliminate the water in the pores by sublimation. Before the MIP tests the samples were heated to 35°C for 2 h. The porosimeter used was a Micromeritics AutoPore Series IV 9500, which allowed the exploration of pore diameters between 0.006 and 600 µm. Prior to mercury injection the sample was outgassed by applying a vacuum of 50 µm-Hg. Afterwards the mercury injection pressure was increased from 2.7 kPa to 220 MPa in 109 steps. To determine the extrusion branch of the curve, the pressure was released in 56 steps down to a pressure of 68.6 kPa. A contact angle of mercury of 139° both on advancing and of receding on the clay surface was considered.

After the determination of the water retention curves a fragment of each sample was used for measuring the pore size distribution following the same methodology just described.

The mercury intrusion method allows access to be gained only to the macroporosity and to part of the mesopores (those of sizes in the range from 50 to 6 nm), since mercury does not intrude the microporosity (pores with diameters of less than 2 nm, according to the classification of Sing et al. 1985). In the high-density clay materials retrieved from the FEBEX-DP, pores larger than those that can be quantified by MIP are not expected. However, the pores connected to the external surface by narrow openings will not be intruded until sufficient pressure is applied to intrude the entryways. All of the volume of such pores will be allocated to the threshold radius class of the most restricted part of the entryway (bottleneck effect).

4.5. Water retention curves

The water retention curves (WRC) were determined with the aim of checking the effect of prolonged drying on the water retention capacity of the bentonite. For this reason, samples from the internal ring of the barrier in contact with the liner were tested. The three blocks received that had been in contact with the liner in sections S47 and S53 were sampled, but also two blocks close to the axis of the gallery in cool section S59 (Fig. 10, Tab. 1). These two blocks had water contents close to those blocks taken from sections S47 and S53, and were sampled to check the effect of the thermal treatment on the water retention capacity, since the blocks from sections S47 and S53 were submitted to much higher temperatures during operation than those from section S59 (Fig. 5). Two samples were obtained by drilling from each block with a crown drill bit of internal diameter 4.5 cm. In the blocks from section S47 these two samples were drilled at two different distances from the axis of the gallery, 1 and 2, as shown in Fig. 14. In the rest of the blocks the two subsamples, a and b, were drilled at the same distance from the gallery axis. The cores obtained were trimmed with cylindrical cutters to adjust their diameter to 3.8 cm and pushed into stainless steel rings which were the body of a cell (Fig. 16, left). The height of the resulting bentonite cylinders varied between 1.1 and 1.3 cm. Filter papers and porous stones were placed on top and bottom of the sample and the covers of the cell were tightened. The cells were placed in desiccators with sulphuric acid solutions (Fig. 16, right), to apply a given suction to the samples by means of the control of the relative humidity (vapour transfer technique). The relative humidity inside the desiccators is related to total suction through Kelvin's equation (Eq. 2).

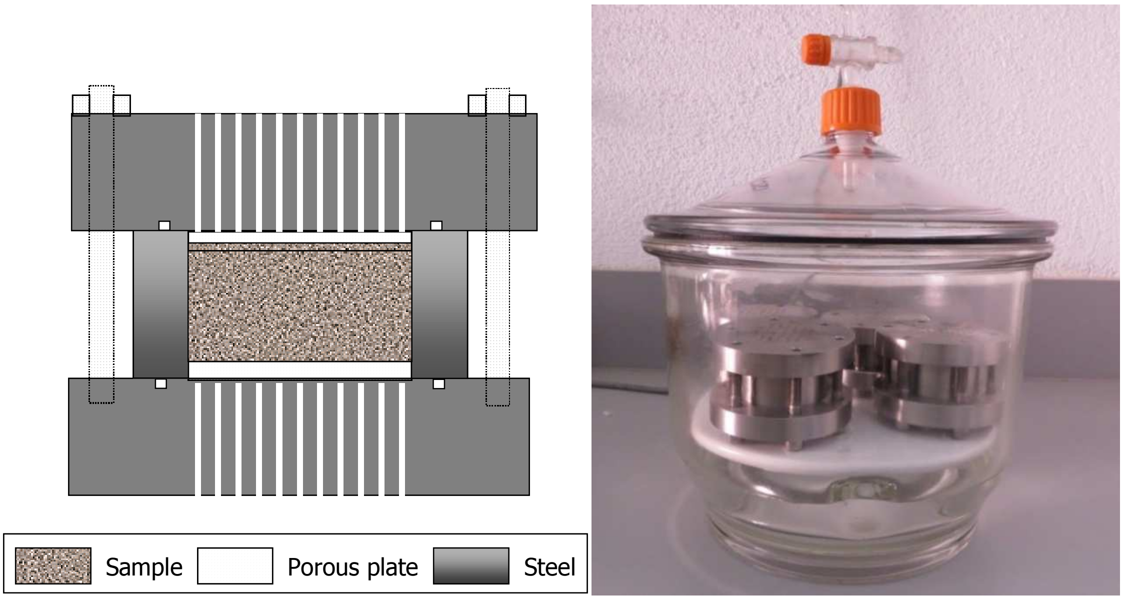

Fig. 16: Schematic representation of the constant volume cell for WRC determination (left) and desiccator with perforated cells inside (right)

The samples were initially submitted to suctions of 19-23 MPa, which were the suctions measured in the blocks following the procedure described in section 4.1. Afterwards, the samples were submitted to suctions progressively lower. The evolution of water content in the samples was checked by periodical weighing, and the suction step was not changed until stabilisation was reached. Once equilibrium was reached for the final suction value, the cells were opened, the samples were extracted by pushing with a hydraulic press and they were weighed and their dimensions measured. Small parts of the samples were used for measurement of the basal spacing and determination of the pore size distribution according to the procedures described in 4.3 and 4.4. All the remaining part of the samples was used for water content determination.

The final density of the sulphuric acid solution in the desiccator was checked using a Density Meter (A-110M-Mettler Toledo, ±0.0001 g/cm^3 resolution). There is an experimental relation between the density of the solution (ρ, g/cm^3) and the percentage in weight of the sulphuric acid in the solution (p, %), which is temperature-dependent (Lide 1995). For 20°C, this relation may be adjusted to an exponential equation:

$$p = 145.8984 \ln \rho + 0.9807 \quad [3]$$

In turn, the relation between the percentage in weight of sulphuric acid in the solution (p, %) and the activity of the solution (a_w=RH/100) –which gives suction according to Kelvin's law (Eq. 2)– is reflected in experimental tables for different temperatures (Gmitro & Vermeulen 1964). For 20°C, the relation may be adjusted to a polynomial equation of the fourth order:

$$a_w = 7 \cdot 10^{-8}\, p^4 - 6 \cdot 10^{-6}\, p^3 - 0.0001\, p^2 - 0.0019\, p + 0.9927 \quad [4]$$

The lowest suction value applied was 0.47 MPa, corresponding to a RH of 99.67% (Eq. 2). This RH was generated using a 10^{-4} M NaCl solution (Clarke & Glew1985).

The determinations were performed at 20°C.

5. Results

5.1. Computation of degree of saturation

The water degree of saturation of the bentonite (S_r), which is the ratio of volume of water to volume of voids, has been computed using the Equation:

$$S_r = \frac{w \times \rho_d}{n} \quad [5]$$

where w is the water content, ρ_d is the dry density, and n is the porosity of the bentonite, in turn computed using the dry density and the solid specific weight (γ_s). This Equation assumes that the water has a density of 1 g/cm^3. The degree of saturation obtained will depend thus on the solid specific weight used. If a value lower than the actual one were used, the degrees of saturation would be fictitiously high and *vice versa*. For the FEBEX bentonite used to manufacture the blocks placed at the GTS, a solid specific weight for the solids component of 2.70±0.04 g/cm^3 (average of 20 measurements) was determined in pycnometers using water for soil suspension (Villar 2002, ENRESA 2000, 2006). In 22 samples taken from Grimsel during the 2015 dismantling, this parameter was determined again and the same average value was found (Villar et al. 2018b).

In addition to the uncertainties in the specific weight value determination, there is another reason for computing inaccurate degrees of saturation. This is the assumption that the density of the water is 1 g/cm^3, although it is known to be higher in the water adsorbed in bentonites. This fact becomes more evident in highly compacted expansive clays close to water saturation, in which degrees of saturation much higher than 100% can be computed if a water density value of 1.0 g/cm^3 is considered (Villar 2002, Marcial, 2003, Lloret & Villar, 2007). Thus, a computed degree of saturation of 115% for a saturated sample would indicate that the average density of the water in it is 1.15 g/cm^3. Besides, the proportion of adsorbed water (with a density higher than 1 g/cm^3) over free water (with a density of 1 g/cm^3) increases as the dry density of the bentonite is higher.

Since there is no accurate knowledge of the values that the density of water can take (which would depend on the particular bentonite, its density and water content), the customary value of

1 g/cm^3 has been used in the calculations presented in the following subchapters, which would partially explain the degrees of saturation higher than 100% found in some cases.

5.2. Basic properties

The blocks were sampled in the laboratory for water content and dry density, which were determined in two (three in some cases) different positions of each block along a radius (named 1 and 2, Fig. 14). The values of water content (*w*), dry density (ρ_d) and degree of saturation (S_r) obtained for the blocks used for the WRC determinations are shown in Tab. 3. The Table also shows the total suction and basal spacing (*d*(001)) measured in the same positions (Villar et al. 2018b).

Tab. 3: Summary of properties determined in the blocks used for water retention curve determinations

Block reference	**Distance[a] (cm)**	***w* (%)**	**ρ_d (g/cm^3)**	**S_r (%)**	**Suction (MPa)**	***d*(001) (nm)**
BB-47-3-1	67	22.2	1.65	94	29.2	1.584
BB-47-3-2	57	20.8	1.63	86		1.727
BB-47-6-1	67	19.4	1.65	82	43.5	1.563
BB-47-6-2	57	18.1	1.65	76	49.8	1.674
BB-47-9-1	67	20.0	1.62	81	28.1	1.615
BB-47-9-2	57	20.9	1.65	89	32.5	1.674
BB-53-3-1	67	22.8	1.65	98	22.9	1.574
BB-53-3-2	57	21.9	1.64	91	25.1	1.585
BB-53-9-1	67	20.8	1.66	90	31.3	1.575
BB-53-9-2	57	19.0	1.62	77	35.6	1.574
BB-53-6-1	67	18.7	1.67	81	33.9	1.599
BB-53-6-2	57	18.2	1.65	77	39.9	1.574
BB-59-5-1	15	25.5	1.57	96	18.9	1.639
BB-59-5-2	5	25.3	1.56	94	19.8	1.611
BB-59-14-1	15	25.4	1.58	97	18.5	1.664
BB-59-14-2	5	25.2	1.57	95	20.1	1.645

[a] approximate distance to gallery axis

The water content and dry density obtained in the laboratory for blocks of the different sections sampled are plotted in Fig. 17 to Fig. 19. The water content decreased from the granite towards the inner part of the barrier in all the sections, whereas the dry density increased. In the three radii sampled in every section the changes were similar. In the sections around the heater (S47 and S53) the change along the radii was approximately linear. Section S59 was always a cool section and the water content at every point in it was much higher than the initial one (14%).

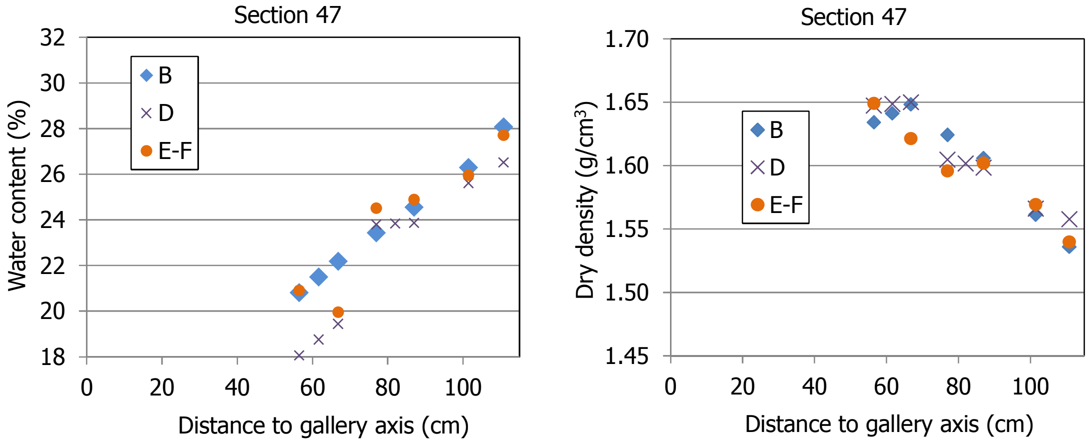

Fig. 17: Water content and dry density measured in the laboratory in blocks taken from section S47 (the sampling radii are indicated in the legend according to Fig. 11)

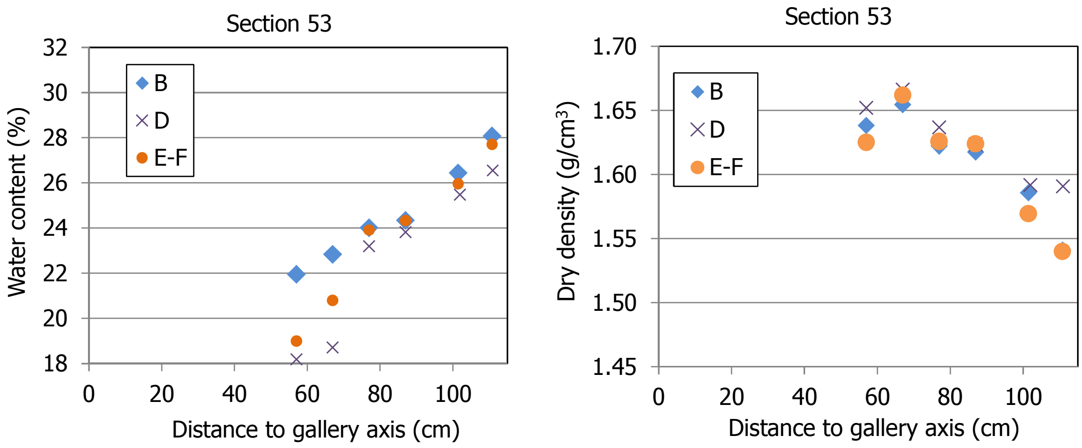

Fig. 18: Water content and dry density measured in the laboratory in blocks taken from section S53 (the sampling radii are indicated in the legend according to Fig. 11)

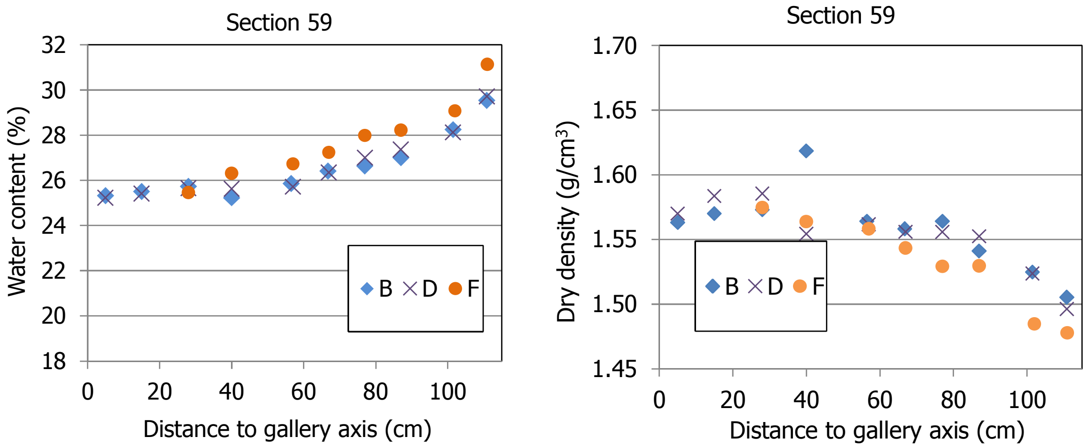

Fig. 19: Water content and dry density measured in the laboratory in blocks taken from section S59 (the sampling radii are indicated in the legend according to Fig. 11)

The results obtained in the laboratory were compared with those obtained on-site by AITEMIN for nearby sections (Villar et al. 2016) and the agreement between both measurements was found to be very good, what suggests that the packing and transport conditions were the appropriate to maintain the *in situ* state of the blocks even several months after their retrieval (Villar et al. 2018b).

5.3. Water retention curve

The samples for the water retention curve determination were obtained by drilling in the laboratory the blocks from sections S47, S53 and S59 indicated in Tab. 1. The exact location of the samples drilled in each section is shown in Fig. 20. They were drilled from blocks in contact with the heater in sections S47 and S53. Samples were also taken from the cool section S59. These samples were trimmed from the most internal blocks of the barrier, which were those with the lowest water content. This was done with the aim of starting the determination of the WRCs from water contents as similar as possible between the two sets of samples (heated and non-heated). Nevertheless, the samples from sections S47 and S53 were drier, and in fact, because of the bad consistency of the blocks, particularly of those from S47 (Fig. 21), it was difficult to obtain good-shaped samples. Because of their higher water content the blocks from section S59 were more consistent and it was easier to trim samples from them (Fig. 22).

After trimming, the samples were placed into perforated cells which were submitted to controlled suctions in desiccators, following the procedure described in subchapter 4.5. The initial suction was selected to be equal to the suction measured in the blocks from which the samples were drilled (Tab. 3), and this suction was subsequently reduced by steps, waiting for water content stabilisation in each step. This way the samples were resaturated and the WRCs were determined following a wetting path under isochoric conditions.

The initial characteristics of the samples from sections S47, S53 and S59 are shown in Tab. 4, Tab. 5 and Tab. 6, respectively. They include the dry density (ρ_d) and water content (w) of the blocks from which they were drilled and the suctions measured in them (those shown in Tab. 3), the initial characteristics of the samples trimmed (ρ_d, w, S_r) and the evolution of these values in the subsequent suction steps. The time necessary to reach water content stabilisation for each step is also indicated. The dry density of the trimmed samples was generally lower than that of the blocks from which they were trimmed, because of the difficulty in trimming samples from blocks that were relatively dry and crumbled easily. There was also a difference between the initial and final dry densities of the samples. This is because the initial height and diameter of the samples –although intended to be as close as possible to the internal dimensions of the cells– did not allow to completely fill the internal volume of the cells, and this was filled in the course of the first suction step, which resulted in a slight increase of the water content of the samples and associated swelling. The subsequent steps brought, as expected, further increases in water content and degree of saturation, since the volume of the samples remained constant during the determination. The evolution of water content as suction decreased for the samples of the different sampling sections is shown in Fig. 23 to Fig. 25. The first suction step brought a decrease in water content for the samples from section S59 –from an average initial water content of 26% to a water content of 24%– whereas for the samples from the other sections the water content slightly increased.

The equilibrium water contents for each suction step are plotted as a function of suction in Fig. 26 to Fig. 28 for the different sections. The initial water contents of the blocks from which the samples were trimmed are also plotted in the Figures linked to the suction measured in the same blocks at the approximate locations where the samples were drilled from (Tab. 3).

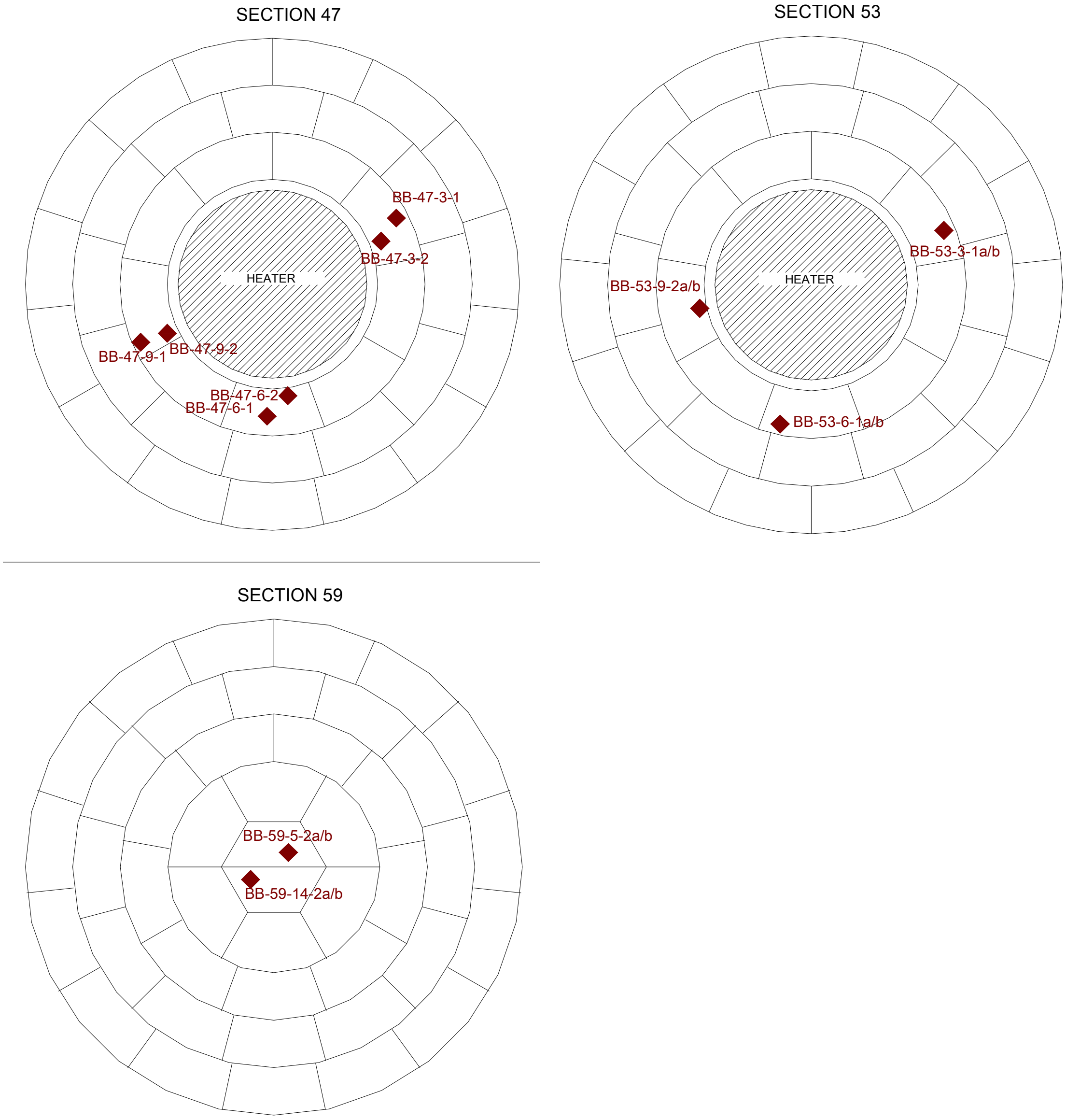

Fig. 20: Location of samples used for water retention curve determination

Fig. 21: Appearance of blocks BB47-3 (up) and BB47-6 (down)

Fig. 22: Appearance of block BB59-5 and location of the two samples trimmed for water retention curves

Tab. 4: Results of the water retention curves with samples from section S47

Reference	1. BB47-9-1	2. BB47-9-2	3. BB47-3-1	4. BB47-3-2	5. BB47-6-1	6. BB47-6-2
Distance to axis (cm)	67	57	67	57	67	57
Block ρ_d (g/cm^3)	1.62	1.65	1.65	1.63	1.65	1.65
Block w (%)	20.0	20.9	22.2	20.8	19.4	18.1
Initial suction (MPa)	28	33	29	29	44	50
Initial ρ_d (g/cm^3)	1.42	1.64	1.68	1.65	1.56	1.54
Final ρ_d (g/cm^3)	1.39	1.52	1.55	1.55	1.50	1.52
Initial w (%)	20.1	20.2	21.1	20.8	18.8	19.9
Initial S_r (%)	60	85	94	88	69	71
Suction (MPa)	23	23	23	23	23	23
Days	49	49	49	49	49	49
w (%)	21.2	21.1	21.8	21.7	20.2	22.5
S_r (%)	61	73	80	79	68	78
Suction (MPa)	13	13	13	13	13	13
Days	105	105	105	105	105	105
w (%)	22.1	22.7	22.8	23.0	21.2	24.4
S_r (%)	63	78	83	83	72	85
Suction (MPa)	11	11	11	11	11	11
Days	198	198	198	198	198	198
w (%)	23.7	24.3	23.8	24.5	22.7	26.8
S_r (%)	68	84	87	89	77	93
Suction (MPa)	6.6	6.6	6.6	6.6	6.6	6.6
Days	113	113	113	113	113	113
w (%)	24.7	24.8	24.2	25.4	23.6	27.9
S_r (%)	71	86	88	92	80	97
Suction (MPa)	0.5	0.5	0.5	0.5	0.5	0.5
Days	291	291	291	228	291	228
w (%)	33.6	31.3	29.1	31.9	30.0	36.3
S_r (%)	96	108	106	115	101	126

Tab. 5: Results of the water retention curves with samples from section S53

Reference	7. BB53-3-1a	8. BB53-3-1b	9. BB53-6-1a	10. BB53-6-1b	11. BB53-9-2a	12. BB53-9-2b
Distance to axis (cm)	67	67	67	67	57	57
Block ρ_d (g/cm^3)	1.65	1.65	1.67	1.67	1.62	1.62
Block w (%)	22.8	22.8	18.7	18.7	19.0	19.0
Initial suction (MPa)	23	23	37	37	33	33
Initial ρ_d (g/cm^3)	1.60	1.57	1.61	1.63	1.58	1.61

Reference	7. BB53-3-1a	8. BB53-3-1b	9. BB53-6-1a	10. BB53-6-1b	11. BB53-9-2a	12. BB53-9-2b
Final ρ_d (g/cm^3)	1.57	1.54	1.56	1.52	1.52	1.57
Initial w (%)	22.2	21.7	19.7	22.4	20.7	19.0
Initial S_r (%)	87	81	79	93	78	76
Suction (MPa)	22.6	22.6	22.6	22.6	22.6	22.6
Days	81	81	76	76	75	75
w (%)	22.3	22.0	20.4	20.9	21.2	19.9
S_r (%)	84	79	75	73	74	75
Suction (MPa)	13.2	13.2	13.2	13.2	13.2	13.2
Days	141	141	141	141	141	141
w (%)	23.4	23.0	21.6	22.1	22.4	21.3
S_r (%)	88	83	80	77	78	79
Suction (MPa)	11.5	11.5	11.5	11.5	11.5	11.5
Days	97	97	97	97	97	97
w (%)	23.9	23.4	22.1	22.5	22.9	21.8
S_r (%)	90	84	81	78	80	81
Suction (MPa)	6.3	6.3	6.3	6.3	6.3	6.3
Days	73	73	73	73	73	73
w (%)	24.2	24.1	22.7	23.4	24.0	22.9
S_r (%)	91	86	84	81	83	85
Suction (MPa)	0.5	0.5	0.5	0.5	0.5	0.5
Days	112	228	228	228	228	112
w (%)	27.2	27.6	27.3	27.5	29.4	25.7
S_r (%)	102	99	101	96	102	96

Tab. 6: Results of the water retention curves with samples from section S59

Reference	13. BB59-14-2a	14. BB59-14-2b	15. BB59-5-2a	16. BB59-5-2b
Distance to axis (cm)	5	5	5	5
Block ρ_d (g/cm^3)	1.57	1.57	1.57	1.57
Block w (%)	25.2	25.2	25.5	25.5
Initial suction (MPa)	20	20	20	20
Initial ρ_d (g/cm^3)	1.54	1.51	1.50	1.53
Final ρ_d (g/cm^3)	1.53	1.48	1.50	1.53
Initial w (%)	26.0	26.1	26.9	23.6
Initial S_r (%)	93	89	91	84
Suction (MPa)	18.7	18.7	18.7	18.7
Days	87	87	87	87
w (%)	23.4	24.7	25.0	21.3

Reference	13. BB59-14-2a	14. BB59-14-2b	15. BB59-5-2a	16. BB59-5-2b
S_r (%)	82	81	84	75
Suction (MPa)	13.4	13.4	13.4	13.4
Days	140	140	140	140
w (%)	24.2	25.4	26.0	22.4
S_r (%)	85	84	88	79
Suction (MPa)	11.5	11.5	11.5	11.5
Days	97	97	97	97
w (%)	24.7	26.0	26.5	22.6
S_r (%)	87	85	89	80
Suction (MPa)	6.5	6.5	6.5	6.5
Days	73	73	73	73
w (%)	25.8	27.2	27.6	23.9
S_r (%)	91	89	93	85
Suction (MPa)	0.5	0.5	0.5	0.5
Days	112	112	291	112
w (%)	29.0	31.0	33.4	27.1
S_r (%)	102	102	113	96

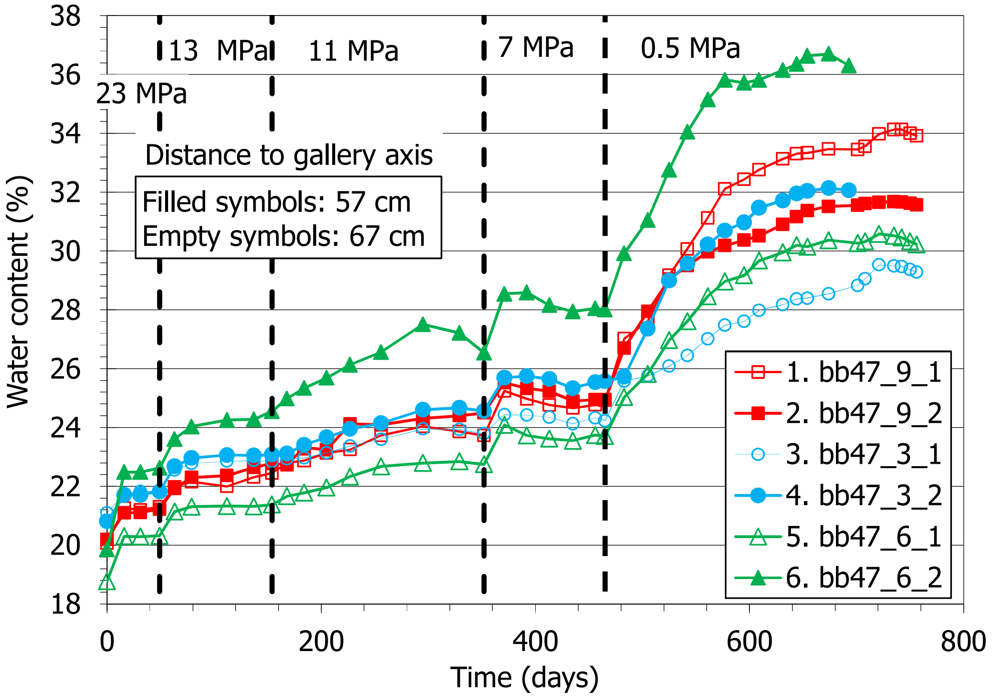

Fig. 23: Water content evolution as suction decreased for samples of section S47 (the vertical lines indicate the suction changes, the suction of each step is indicated in the upper part)

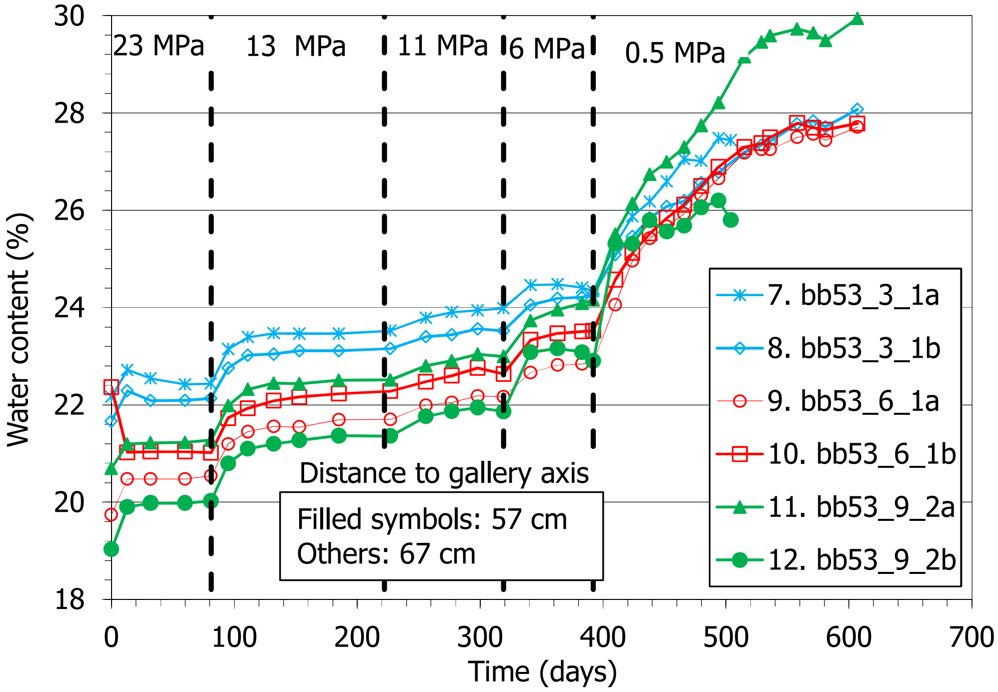

Fig. 24: Water content evolution as suction decreased for samples of section S53 (the vertical lines indicate the suction changes, the suction of each step is indicated in the upper part)

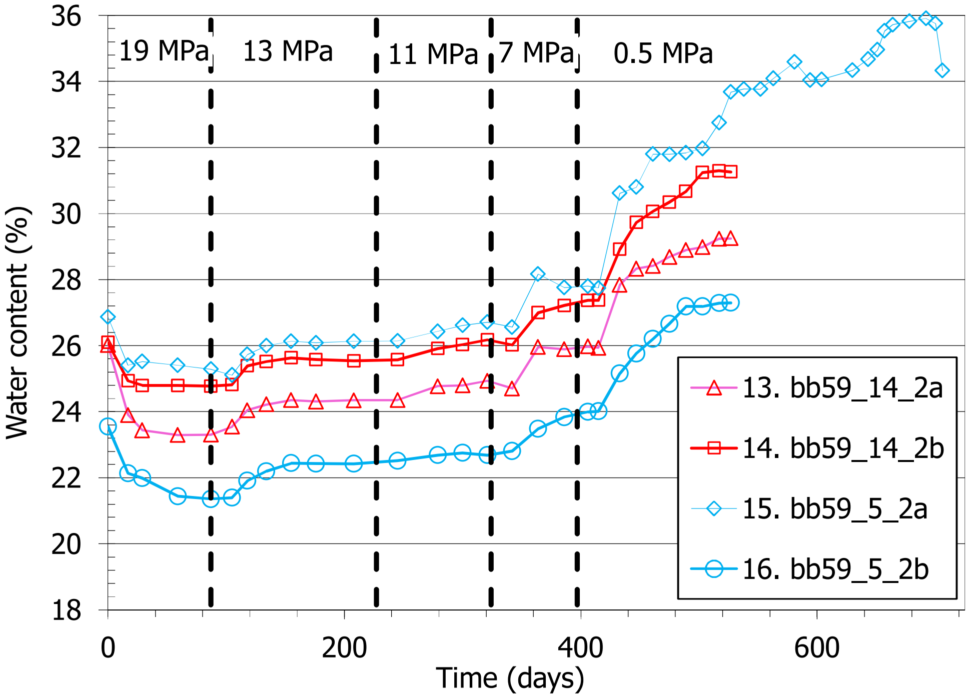

Fig. 25: Water content evolution as suction decreased for samples of section S59 taken at 5 cm from the gallery axis (the vertical lines indicate the suction changes, the suction of each step is indicated in the upper part)

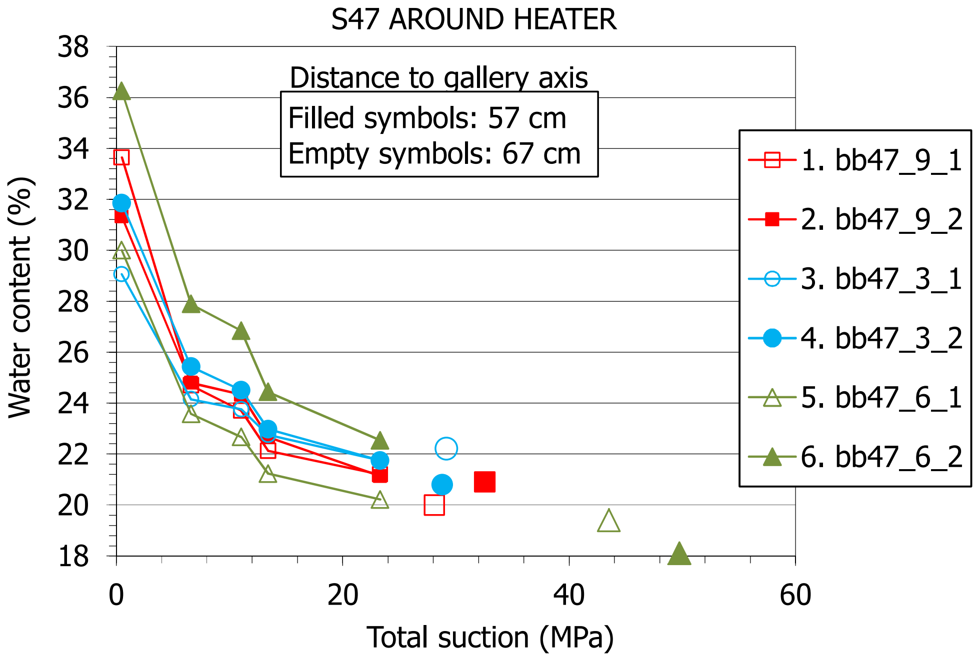

Fig. 26: Water retention curves determined for samples of section S47. The highest suction value for each sample (largest symbols) is that measured in the block from which it was trimmed and reported in Tab. 3

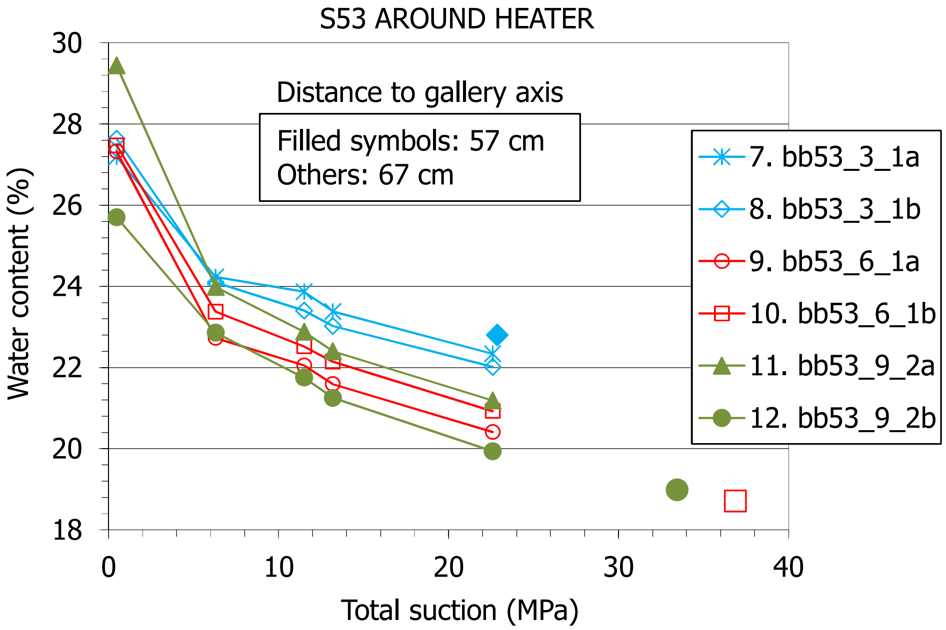

Fig. 27: Water retention curves determined for samples of section S53. The highest suction value for each sample (largest symbols) is that measured in the block from which it was trimmed and reported in Tab. 3

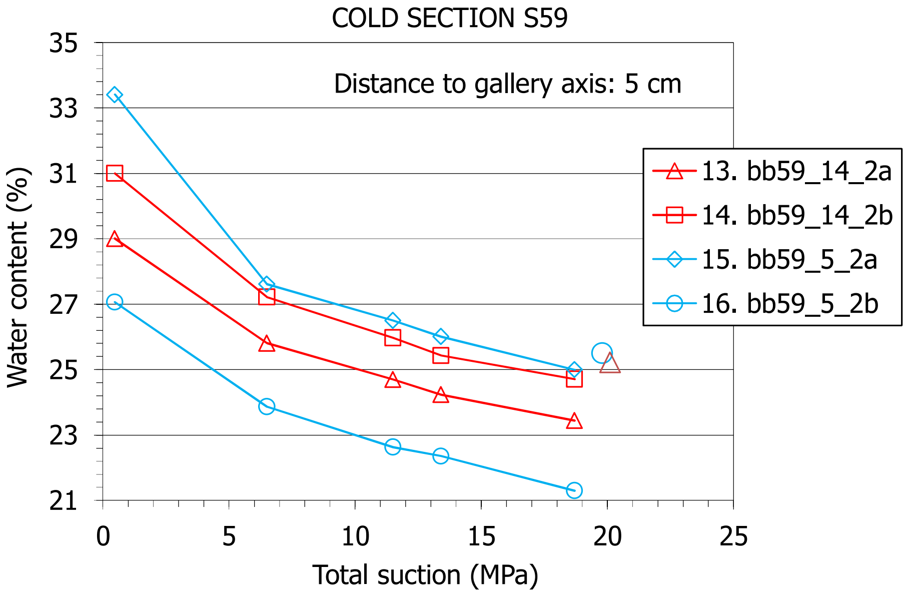

Fig. 28: Water retention curves determined for samples of section S59. The highest suction value for each sample (largest symbols) is that measured in the block from which it was trimmed and reported in Tab. 3

These Figures show that even inside the same block, the behaviour of the samples was different. A possible explanation is the wide range of variation in dry densities, which spanned between 1.39 and 1.58 g/cm^3, since dry density has an effect on the water retention capacity, particularly for the lowest suctions. However, in the results for the FEBEX-DP samples just presented this relation was not clear and the divergence between samples cannot be explained by their different dry densities. In contrast, the initial water content seems to also have a significant influence on the water content evolution during wetting, particularly for suctions above 10 MPa. This means that the initial water content difference between samples was more or less preserved until suction reached values around 10 MPa: samples with higher initial water content kept having higher water contents than the other samples during the wetting path. But when suction decreased below 10 MPa the trend changed.

Additionally, the samples have been grouped according to their position in the barrier, particularly their distance to the gallery axis, which in the samples around the heater conditioned the maximum temperature to which they were submitted. The results for the samples that were taken closer to the heater, i.e. at 57 cm from the gallery axis in sections S47 and S53, have been plotted in Fig. 29. Since section S47 was located in the middle part of the heater whereas section S53 was towards the back of it, the temperatures during operation were very likely higher in section S47 (Fig. 5). However, the initial water contents were higher for the samples from section S47, and they kept so during the whole wetting path, the difference with the samples from section S53 increasing as suction decreased. The results for the rest of the samples, i.e. those taken at 67 cm from the gallery axis in sections S47 and S53, and from cool section S59 are plotted in Fig. 30. In this case the initial water contents of samples from sections S47 and S53 were similar, but wetting for suctions below 10 MPa resulted in a higher increase in water content for the samples of section S47. In fact, although the samples from section S59 had higher initial water contents than the rest of the samples, the final water contents at the end of the wetting path were similar for the two sets of samples (S47 and S59). It could be concluded that the samples submitted to the highest temperatures (above 90°C according to Fig. 4) had for the lowest suctions the highest water adsorption capacity.

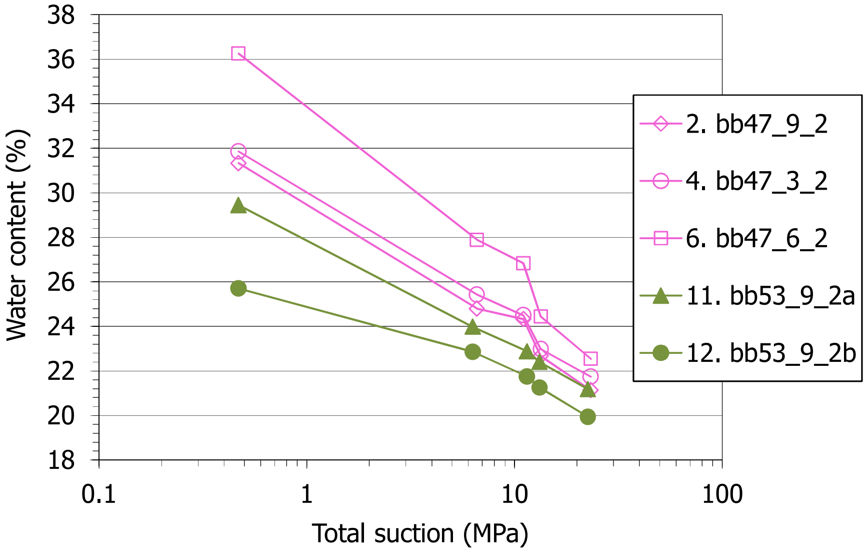

Fig. 29: Water retention curves of samples located at 57 cm from the gallery axis in sections S47 and S53

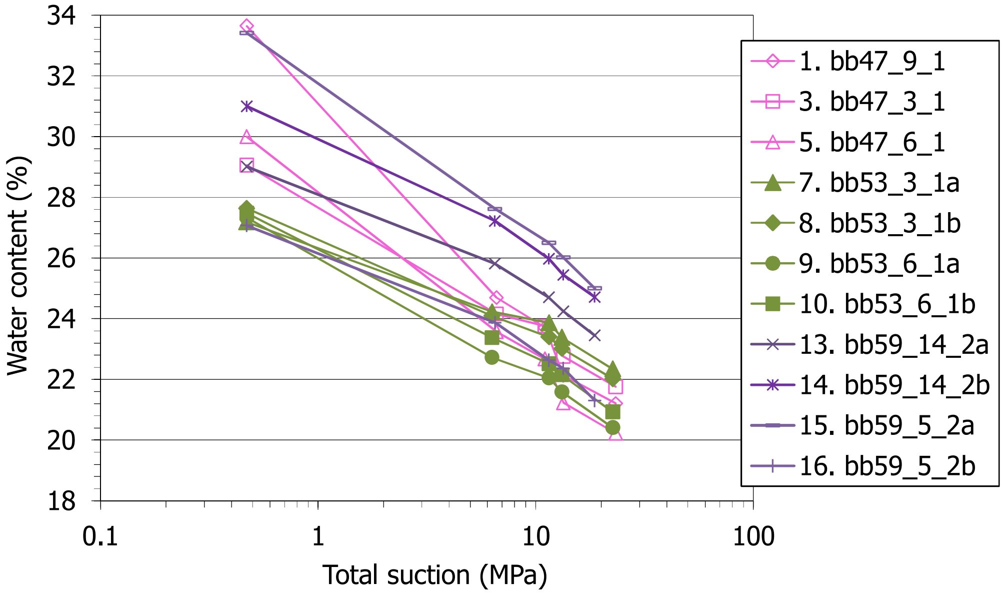

Fig. 30: Water retention curves of samples located at 67 cm from the gallery axis in sections S47 and S53 and 5 cm from the gallery axis in section S59

5.4. Pore size distribution of tested samples

The pore size distribution of the samples at the end of the WRC tests was analysed by mercury intrusion porosimetry. The equipment used could get access to pores of diameters in the range from 540 µm to 7 nm. Fig. 31 to Fig. 33 show the curves obtained for the samples from the three sampling sections. The curves have been filtered with the Savitzky-Golay's method (1964) to remove the experimental noise. Two pore families appeared systematically in all the samples, one in the size range of macropores and another one in the size range of mesopores. This is the usual pore size distribution pattern obtained by MIP in compacted FEBEX bentonite, irrespective of the water content or dry density, and was also observed in the samples taken from the FEBEX-DP blocks and not used for WRC determination (Villar et al. 2018b).

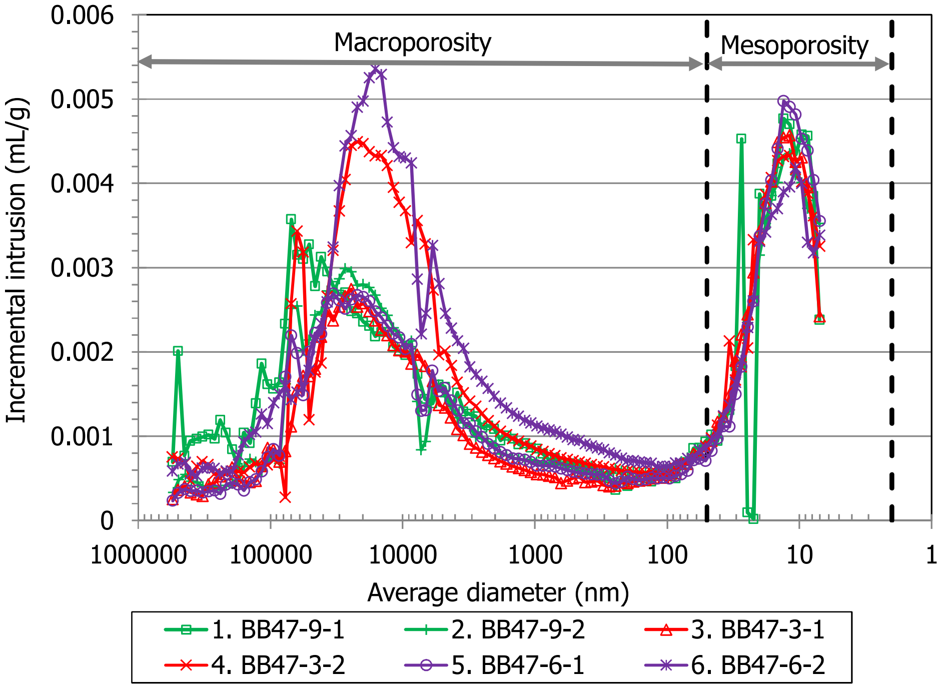

Fig. 31: Pore size distribution obtained by MIP of samples from section S47 after WRC determination

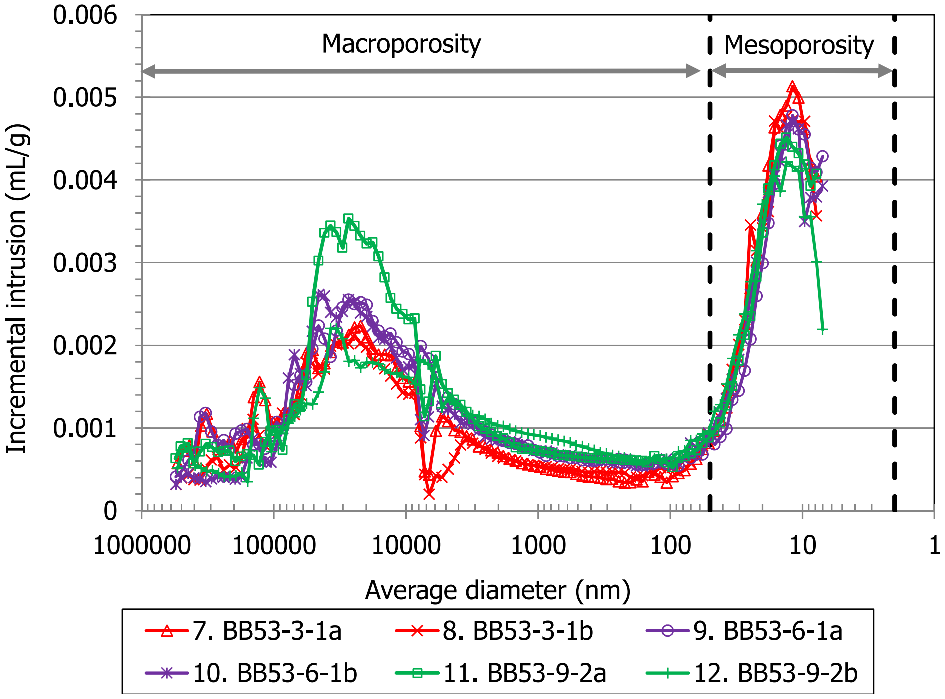

Fig. 32: Pore size distribution obtained by MIP of samples from section S53 after WRC determination

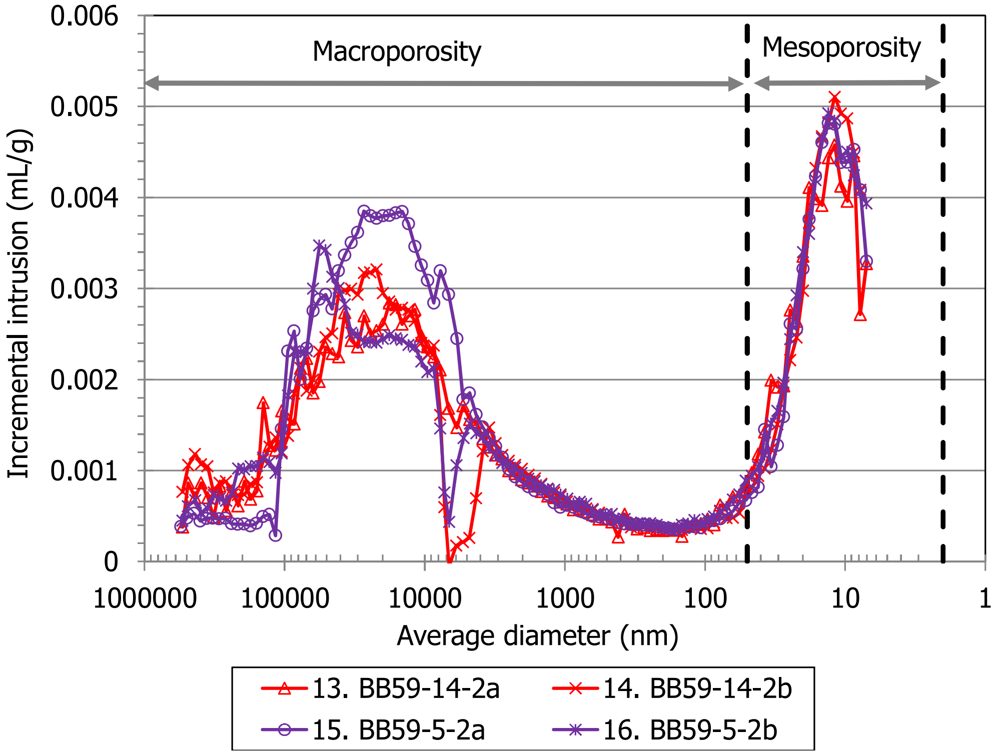

Fig. 33: Pore size distribution obtained by MIP of samples from section S59 after WRC determination

Because of the limitations of the method and equipment, only part of the macropores (pores of diameter in the range from $5.4 \cdot 10^5$ to 50 nm) and part of the mesopores (pores of diameter between 50 and 7 nm) were explored. It is not expected to find pores larger than $6 \cdot 10^5$ nm in compacted clay materials, but the number of pores smaller than 7 nm can be very relevant. To overcome this undervaluation of porosity, an estimation of the percentage of pores not intruded by mercury can be made by comparing the actual void ratio of the samples (e, computed from their dry density in Tab. 4 to Tab. 6, and the density of solid particles) and the apparent void ratio calculated from mercury intrusion (e_{nw}, mercury being a non-wetting fluid) and assuming that the non-intruded porosity corresponds to the pores of a size smaller than the limit of the apparatus. Thus, the pore size distribution obtained by MIP was corrected to take into account the percentage of pores not intruded.

The corrected results are detailed in Tab. 7. The non-intruded void ratio was between 50 and 74%. The Tables also show the void ratio corresponding to macropores (diameter >50 nm), mesopores (7 nm < diameter ≤50 nm) and micropores (i.e. those of diameter <7 nm), along with the size mode of macropore and mesopores. The separate quantification of mesopores and micropores cannot be accurately done, because the diameter limit of the two pore sizes is 2 nm, whereas the lower limit of the equipment is 7 nm. No differences in the parameters mentioned have been detected between the samples of the three sections.

Tab. 7: Pore size distribution of the bentonite obtained by MIP after determination of the WRC (sizes correspond to diameters)

Reference	***e***	**Intruded *e* (% total)**	***e* macro (>50 nm)**	**Mode macro (nm)**	***e* meso (50-7 nm)**	**Mode meso (nm)**	***e* micro[a] (<7 nm)**
1. BB47-9-1	0.944	50	0.323	69674	0.150	13.2	0.471
2. BB47-9-2	0.780	55	0.279	69555	0.152	11.9	0.349
3. BB47-3-1	0.738	54	0.244	27147	0.155	13.2	0.339
4. BB47-3-2	0.745	70	0.366	62865	0.155	13.2	0.224
5. BB47-6-1	0.799	53	0.263	69662	0.159	13.2	0.376
6. BB47-6-2	0.779	74	0.431	16081	0.145	10.7	0.203
7. BB53-3-1a	0.718	57	0.235	24428	0.172	10.7	0.311
8. BB53-3-1b	0.752	50	0.210	24593	0.167	10.7	0.375
9. BB53-6-1a	0.731	58	0.271	30145	0.156	10.7	0.304
10. BB53-6-1b	0.776	54	0.256	45844	0.160	7.8	0.360
11. BB53-9-2a	0.769	60	0.308	37211	0.161	11.9	0.308
12. BB53-9-2b	0.722	56	0.252	33417	0.153	11.9	0.317
13. BB59-14-2a	0.764	59	0.291	17853	0.156	11.9	0.316
14. BB59-14-2b	0.822	55	0.291	24433	0.163	10.7	0.368
15. BB59-5-2a	0.706	70	0.339	14484	0.157	13.2	0.210
16. BB59-5-2b	0.763	61	0.297	56387	0.166	14.6	0.300

[a] assuming that all the non-intruded porosity corresponds to pores <7 nm

The pore size distribution of samples from the blocks from which the samples for the WRC determination were trimmed was also analysed when the blocks were first sampled. The results were reported in Villar et al. (2018b). Those results are plotted in Fig. 34 in terms of void ratio corresponding to pores with diameters larger and smaller than 50 nm (i.e. macropores and meso+micropores, respectively) for samples taken at different distances from the heater in sections S47 and S53. The results obtained after the WRC determination in samples taken from close positions (Tab. 7) have also been plotted in the Figure. There is an overall increase in void ratio after the WRC determination, which has been explained above as caused by the difficulties in trimming samples that perfectly fit the testing cells, what gave place to reductions of dry density after trimming. Both the percentage of void ratio of pores larger and smaller than 50 nm increased after the WRC testing, i.e. after the samples were resaturated, but the percentage of macropores increased proportionally more. The same information has been plotted in Fig. 35 for the samples taken from section S59: the void ratio corresponding to pores larger and smaller than 50 nm before and after the WRC determination are compared. In addition to the overall higher void ratio of the samples trimmed for the WRC tests, the increase was again proportionally higher for the pores with diameters larger than 50 nm. In fact, the average percentage of void ratio corresponding to pores smaller than 50 nm for all the samples in which the WRC was determined was 62±7%, whereas it was 68±2% for the samples taken from the blocks and not tested. This would mean that the resaturation occurred during the WRC determination resulted in an increase mainly of macropores.

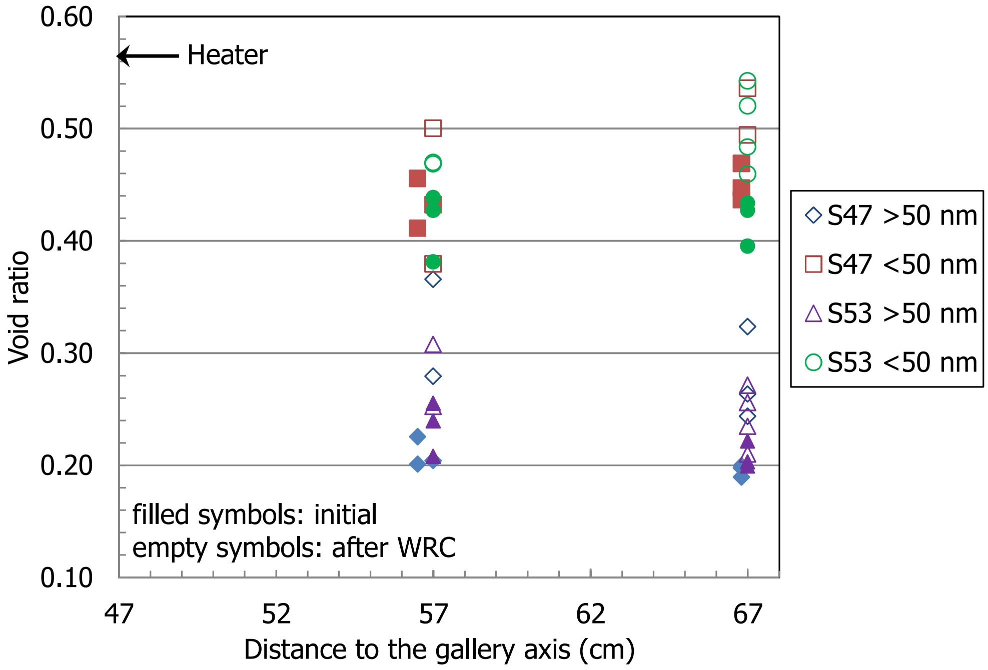

Fig. 34: Change in void ratio distribution during the WRC determination in samples taken at different distances from the heater in sections S47 and S53

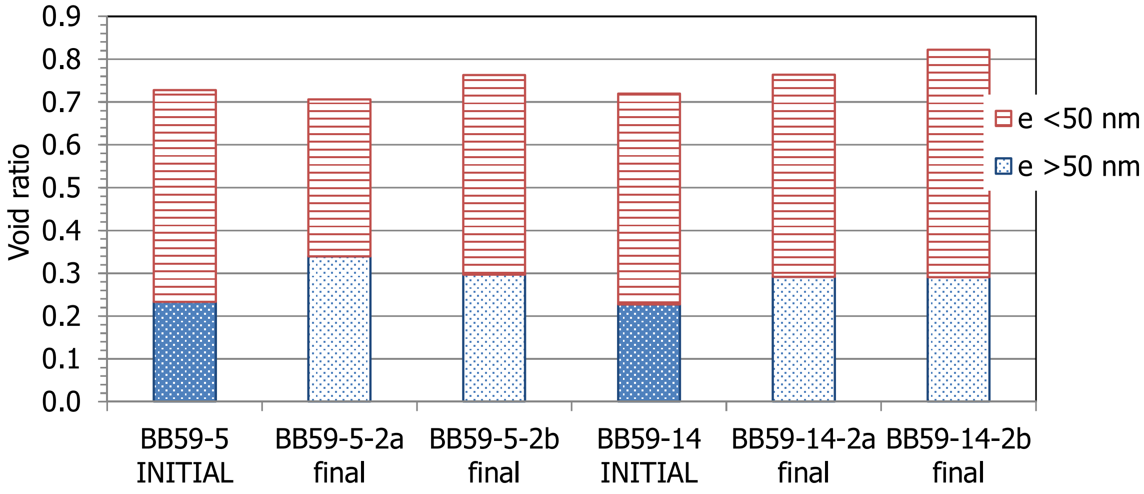

Fig. 35: Distribution of void ratio in samples taken at 5 cm from the gallery axis in section S59 before and after the WRC determination

5.5. Interlayer space of tested samples

The basal spacing of the samples after the WRC determination was determined by XRD according to the procedure described in 4.3. Fragments of the samples were X-rayed the same day in which the cells were dismantled, trying to keep the final water content unchanged by avoiding any accidental drying. This analysis was also performed in samples from the blocks when they were first sampled in the laboratory, and the results obtained were shown in Tab. 3 (Villar et al. 2018b). The new results obtained after the determination of the WRC are plotted in Fig. 36 as a function of the distance to the gallery axis and compared with the values measured in samples from the same blocks before the WRC determination (Tab. 3). The 001-reflection peak was in fact a double one that could be decomposed into two peaks by profile fitting of the XRD patterns. The main peak, which is the one plotted in the Figure, was comprised between 1.50 and 1.74 nm (1.59±0.05 nm) and the secondary one between 1.77 and 2.17 nm (1.94±0.13 nm), the main peak corresponding to the full development of the 2-layer hydrate and the secondary one to the 3-layer hydrate. Double peaks were also observed in most untested block samples.

These values are plotted in Fig. 37 as a function of the water content of the samples. Since the water content increased during the determination of the WRC, the basal spacings also increased, both the values for the main and for the secondary peaks, but particularly the secondary one. The results obtained after the WRC determination have been plotted again as a function of the water content in Fig. 38, along with values measured in FEBEX bentonite samples after swelling pressure tests, i.e. in samples saturated with liquid water under isochoric conditions (Villar et al. 2012 and unpublished results). The values obtained after the WRC curve fit in the range expected for saturated samples of the same dry density, what would indicate that the distribution of water in the microstructure of the tested retrieved samples is the expected for the untreated, reference FEBEX bentonite.

Although the analyses for the two set of samples (tested in the laboratory for WRC and non-tested blocks) were performed with different apparatuses (subchapter 4.3), no effect on the results obtained has been identified.

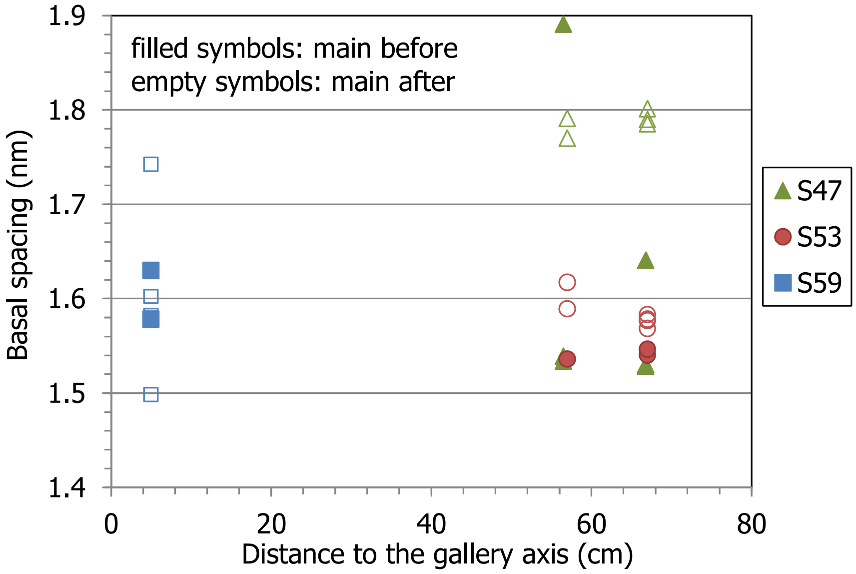

Fig. 36: Change in main peak of the basal spacing reflection of samples taken from different sampling sections during the WRC determination

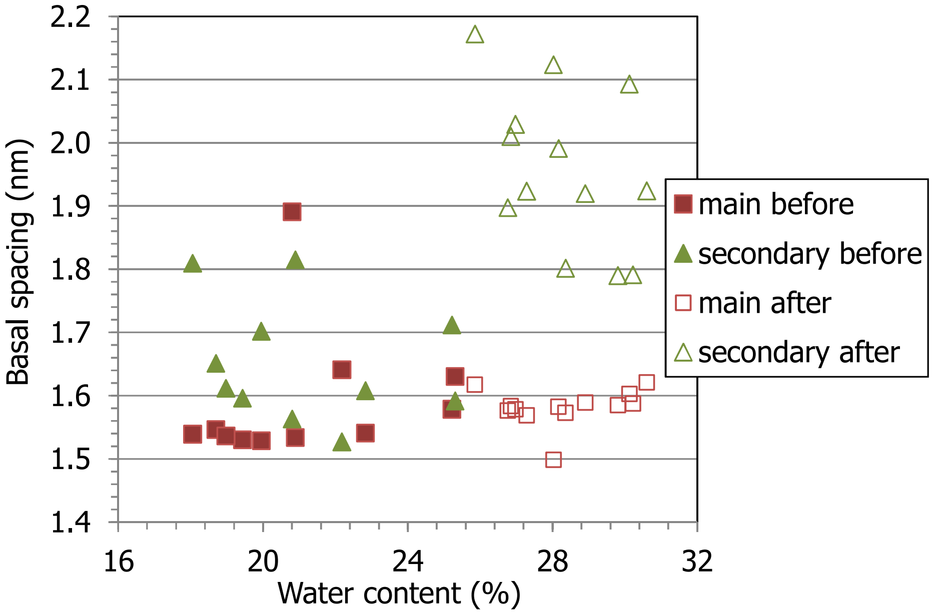

Fig. 37: Main and secondary peaks of the basal spacing reflection of samples after the WRC determination and of non-tested samples taken from the same positions

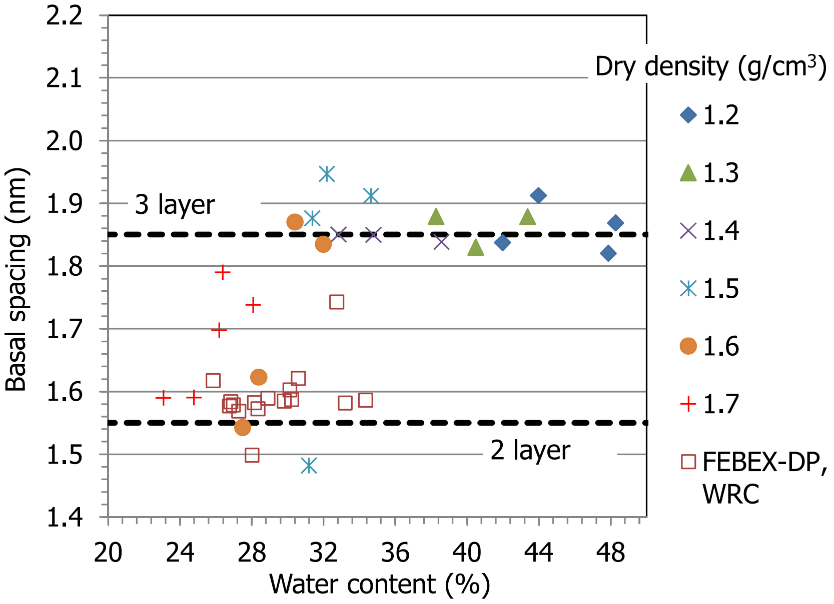

Fig. 38: Main basal spacing of FEBEX samples after swelling pressure tests (Villar et al. 2012 and unpublished results) and for the FEBEX-DP samples after WRC determination

6. Discussion

The water retention capacity of a material depends on its mineralogical composition –which is assumed to be the same in all the FEBEX-DP samples, since no relevant mineralogical changes were observed (Fernández et al. 2018)–, the hydraulic path (drying paths resulting in higher water contents than wetting paths), the temperature, the dry density and the stress conditions (both aspects particularly relevant in expansive materials). Other factors such as the salinity of the water available or the nature of the exchangeable cations may also affect the water retention capacity of a bentonite. Some of the influencing factors were not reproduced in the laboratory determinations, such as the temperature (which for some of the samples tested was higher during operation, whereas it was kept at 20°C during the laboratory determinations), kind of available water (particularly its salinity, since water was taken by the samples in the laboratory in the vapour phase) or the precise stress conditions (which were isochoric in the laboratory tests, whereas the barrier was submitted to different stresses). For these reasons, the aim of the tests reported here was not to define the WRC of the samples as when they were in the barrier during operation, but to check if the material retrieved had the same water retention capacity that could be expected for the FEBEX reference bentonite under similar conditions (temperature, dry density and hydraulic path). Hence, all the factors possibly affecting the results have to be analysed before assessing the preservation of the water retention capacity.

The samples from sections S47 and S53 had a hydraulic history different to those from cool section S59, since the former had been dried during operation whereas the latter had been continuously wetted. Hence, the determination of the water retention curve for samples from sections S47 and S53 followed a “wetting after drying” path, whereas the samples from section S59 continued in the laboratory the wetting path started in the barrier (although in fact the first step of the WRC determination resulted in a slight drying). It is acknowledged that the water retention process is affected by hysteresis, and that for a given suction higher water contents are reached during drying than during wetting. In this sense, it would be logical to find differences between the water retention curves of the samples from cool section S59 and the sections around the heater submitted to intense drying during operation. The results shown in subchapter 5.3 have been plotted again in Fig. 39, grouped according to the hydraulic history of the samples and for dry density intervals. The fact that there was a broad range in the dry density of the specimens tested makes it difficult to analyse the results, since the dry density probably had also an influence on the water contents reached for each suction. Nevertheless it seems that the samples from section S59 reached overall higher water contents, except maybe for the lowest suctions.

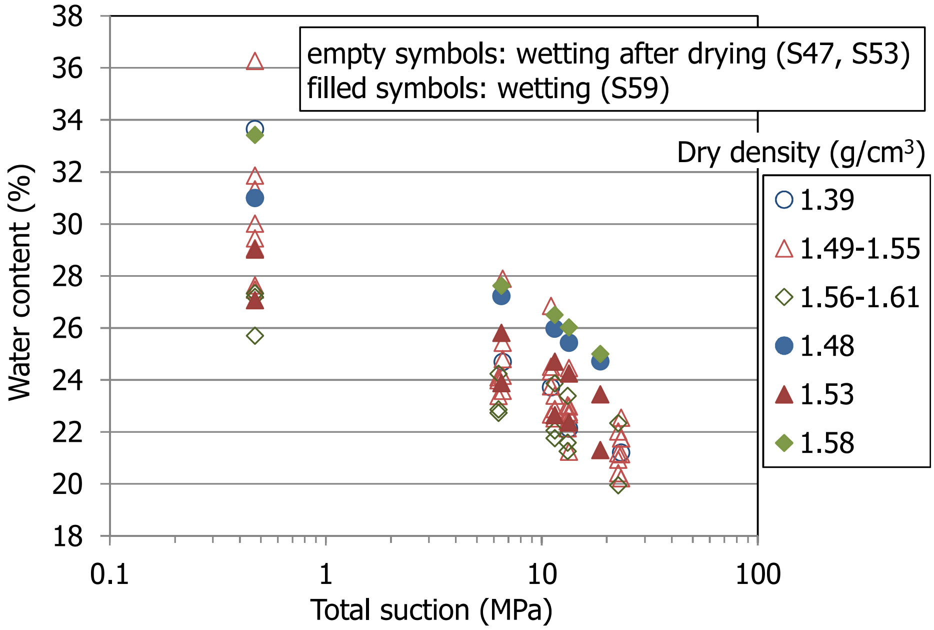

Fig. 39: Water retention curves of samples from different sections grouped according to their dry density and hydraulic path

In an attempt to clarify this matter, the average values for the two kinds of samples (heated during operation and not heated) have been plotted in Fig. 40, along with some other values that allow completing the hydraulic history of the samples:

- The beginning of the drying branch is considered to be the condition of the material in the geological deposit (the Cortijo de Archidona quarry). A tentative value of 40% has been taken based on the water content of bentonite samples obtained by drilling at the quarry (Villar et al. 1996).
- At the factory the bentonite was softly dried until reaching the water content with which the blocks were manufactured, 14%, which corresponds to the equilibrium value under an approximate suction of 100 MPa (ENRESA 2006).
- During operation the relative humidity close to the heater (sections S47-S53) decreased to values of 10% (AITEMIN 2002), which taking into account the temperature in the area (Fig. 4) would correspond to suctions close to 400 MPa. According to the water retention curves of the FEBEX reference bentonite the water content corresponding to this suction could be around 6% (Villar & Gómez-Espina 2009).
- From this value on the bentonite slowly hydrated during operation. In the case of S59 the water content of the bentonite did not decrease at any moment below 14%.
- When the heater was switched off the temperatures decreased and the suctions and water contents in S47-S53 changed. Since there is no factual information on the magnitude of this change (although in terms of water content the changes were probably limited, because of the high degree of saturation of the barrier), this part of the hydraulic history of the samples has not been included in the Figure.
- Finally, the samples retrieved were subjected in the laboratory to a wetting path (indicated by solid lines in the Figure).

Despite the limitations of these approximations, Fig. 40 shows that the samples in the barrier followed scanning curves starting from different suctions: the samples from the cool section S59 started their wetting from a suction of about 100 MPa (corresponding to hygroscopic conditions), whereas the samples close to the heater started the wetting scanning curve from a much higher suction. This could be the reason why the samples from the cool section S59 reached higher water contents than the others. Towards lower suctions this difference seemed to attenuate.

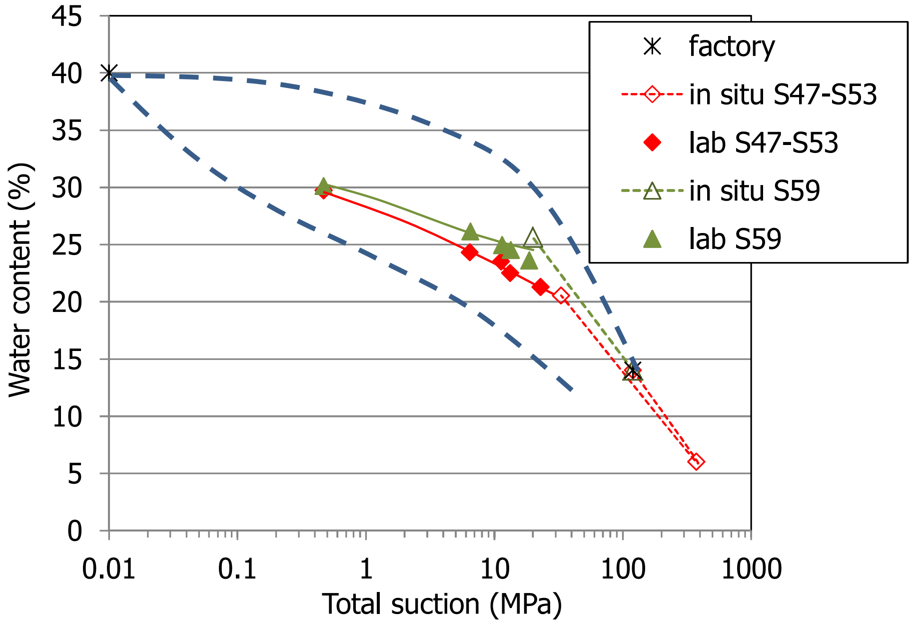

Fig. 40: Hypothetical hydraulic history of the samples used for the water retention curve determination (the filled symbols are the averages of the values reported in subchapter 5.3)

As it was explained in subchapter 4.1 the suction of the blocks was measured in the laboratory before being unpacked. The values obtained were related to the water contents measured in the same samples (Tab. 4 to Tab. 6) and it was possible to draw water retention curves for different ranges of dry density (Villar et al. 2017, 2018b). These results are plotted in Fig. 41 along with the water retention curves shown above. The same ranges of dry density have been considered. The Figure also shows the water retention curve for the FEBEX reference bentonite obtained previously using both methods (sensor measurement and vapour transfer in desiccators) for the same density as the average dry density of the barrier (1.6 g/cm^3). For suctions below 20 MPa the samples of lower density had higher water retention capacity, since their porosity was higher. This was very clear for the results obtained by measuring suction, but could also be stated from the results obtained in cells. For higher suctions the effect of density cannot be evaluated solely based on the results obtained with sensors, because the range of densities was too narrow. As it has been explained above, the effect of density was not clear in the results obtained in cells. However, for suctions above 20 MPa the samples tested in the desiccators (empty symbols) reached lower water contents for a given suction than those measured in blocks of the same suctions (filled symbols).

The comparison with the curve for the reference bentonite compacted to dry density 1.6 g/cm^3 shows that for suctions above 20 MPa the WRCs obtained with sensors were in the range or showed slightly higher retention capacity than the reference bentonite. In contrast, the WRCs obtained in cells showed lower retention capacity (lower water contents for the same suction) than the reference bentonite. This can be explained by the differences in dry density, since the dry densities of the samples tested in cells were mostly below 1.6 g/cm^3 whereas those of the blocks in which suctions higher than 20 MPa were measured were above 1.6 g/cm^3. Experiments performed with the FEBEX bentonite compacted at different dry densities showed that for high suctions the water retention capacity was higher the higher the dry density, although the trend inverted towards lower suctions (Villar 2002).

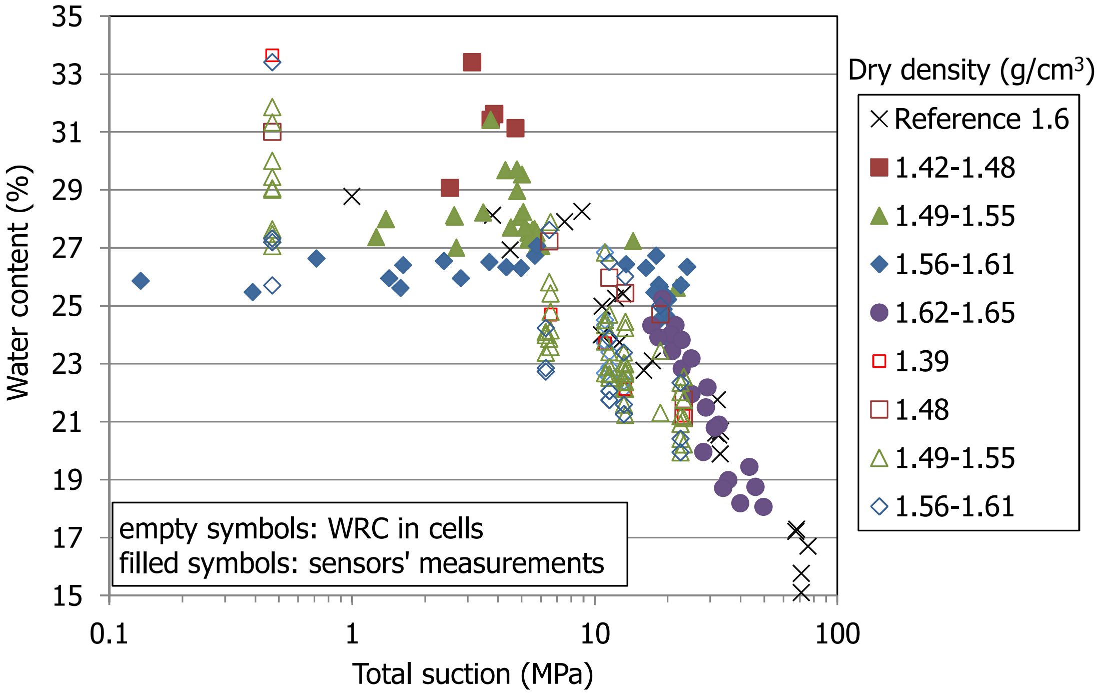

Fig. 41: Water retention curves of the reference bentonite compacted at 1.6 g/cm^3 (crosses), obtained by measuring the suction of blocks with different water content (Villar et al. 2018b, filled symbols) and obtained in cells (this report, empty symbols)

To better evaluate the possible changes occurred in the water retention capacity during operation, the water retention curves obtained in the FEBEX-DP samples have been compared in Fig. 42 with those obtained for the reference bentonite compacted to different dry densities and submitted under confined conditions to different suctions, following the same procedure presented in this report. All the values were obtained in wetting paths (Villar 2007, Villar et al. 2012 and unpublished results). The results of the FEBEX-DP samples have been grouped in dry density ranges close to those available for the reference bentonite. Despite the scatter of the data, it can be said that the water retention capacity did not noticeably change during operation, and certainly it did not decrease.

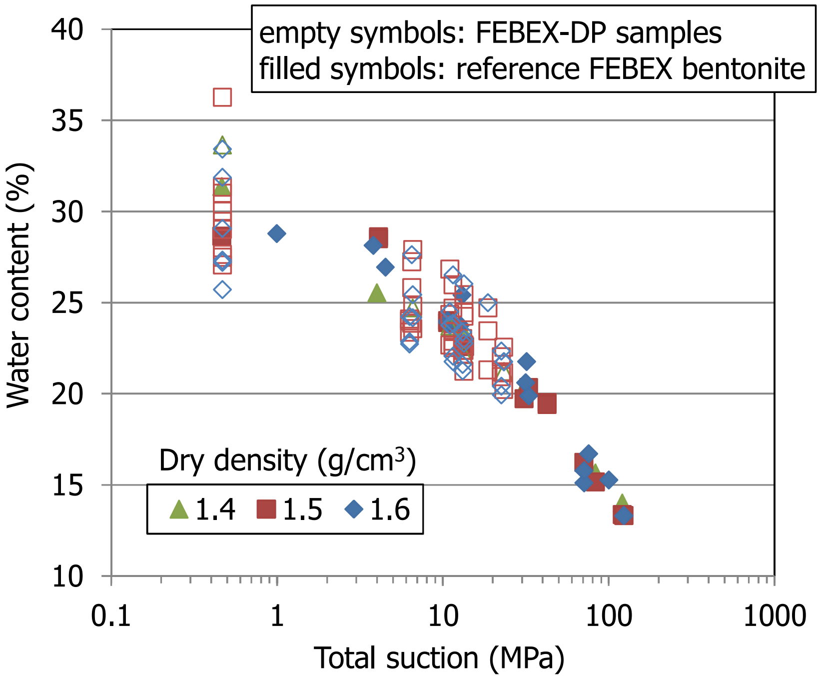

Fig. 42: Water retention curves obtained in cells for the reference bentonite compacted at different dry densities (filled symbols) and for the FEBEX-DP samples (this report, empty symbols)

7. Summary and conclusions

7.1. The FEBEX in situ test

The aim of the FEBEX project (Full-scale Engineered Barriers Experiment) was to study the behaviour of components in the near-field of a repository in crystalline rock according to the Spanish reference concept for geological disposal of nuclear waste. As part of this project an *in situ* test, under natural conditions and at full scale, was performed at the Grimsel Test Site (Switzerland). The heating stage of the test began in 1997. After five years of operation, half of the experiment was dismantled. The remaining part of the experiment continued running until April 2015, when the final complete dismantling of the experiment was undertaken.

At the time of dismantling, spring-summer 2015, the test had been in operation for 18 years. During this time:

- the bentonite barrier was hydrated with the groundwater coming from the granitic host rock, and
- the part of the barrier around Heater #2 –whose surface temperature was 100°C– was submitted to a steep thermal gradient for the entire test. This also means that the internal part of the barrier around the heater was initially strongly dried.

During dismantling numerous bentonite samples, in the form of blocks, cores or irregular fragments, were taken, some of them were analysed on site (water content and dry density determination) and others were carefully vacuum-packed and sent to the different laboratories. These samples are called FEBEX-DP or retrieved samples.

The measurements performed showed that the water content decreased from the granite towards the axis of the gallery whereas the dry density increased. Hence, the void ratio of the samples (inversely related to dry density) was lower the closer to the gallery axis they were taken. Nevertheless, when the heater was switched off and before the blocks were retrieved, the thermal gradient disappeared, and this could trigger some homogenisation of the water content inside the blocks by diffusion.

7.2. Water retention curves determination

This report has focused on the water retention characterisation of the FEBEX-DP samples, in particular on their water retention curves (WRC). The results have been compared with the suction measurements performed with sensors in the retrieved blocks reported in Villar et al. (2018b). At the end of the WRC tests the pore size distribution of the samples was determined by mercury intrusion porosimetry (MIP) and the interlayer distance of the smectite by X-ray diffraction. A summary of the basic characterisation of the blocks from which the samples used for the WRC determination were drilled has also been presented. In particular, results concerning their pore size distribution and interlayer distance have been compared with those obtained for the WRC-tested samples. Additionally, in order to assess the potential changes occurred during operation on the properties investigated, the values obtained have been compared with those of the reference, untreated FEBEX bentonite.

The samples for the water retention curve determination were obtained by drilling in the laboratory the blocks that had been in contact with the heater in sampling sections S47 and S53, since the major aim of the tests was to check if the water retention capacity of the bentonite was affected by long-term drying. Samples were also taken from the cool section S59, to check if there were differences between heated and non-heated bentonite. These samples were trimmed from the most internal blocks of the barrier, which were those with the lowest water content. This was done with the aim of starting the determination of the WRCs from water contents as similar as possible between the two sets of samples (heated and non-heated).

After trimming, the samples were placed into perforated cells which were submitted to controlled suctions in desiccators at a temperature of 20°C (vapour transfer technique, with suction applied by changing the relative humidity inside the desiccator using different chemical solutions). Because of the difficulties in trimming good-shaped samples their dry densities spanned a broad range and were in general lower than the dry densities of the blocks from which they were trimmed. This decrease was not in all cases of the same magnitude, since it depended on the sample conditions and on the operator. The initial suction was selected to be equal to the suction measured in the blocks from which the samples were drilled. The suction in the desiccators was subsequently reduced by steps, waiting for water content stabilisation in each step. This way the samples were saturated and the WRCs were determined following a wetting path under isochoric conditions.

The water retention capacity of a material depends on its mineralogical composition –which is assumed to be the same in all the FEBEX-DP samples, the hydraulic path (drying paths resulting in higher water contents than wetting paths), the temperature, the dry density and the stress conditions (both aspects particularly relevant in expansive materials). Other factors such as the salinity of the water available or the nature of the exchangeable cations may also affect the water retention capacity of a bentonite. Hence, the interpretation of the results obtained is subjected to consideration of the possible changes of the factors affecting the retention capacity occurred during barrier operation and in the laboratory. Some of the factors were not reproduced in the laboratory determinations, such as the temperature, kind of available water or the precise stress conditions. For these reasons, the aim of the tests reported here was not to define the WRC of the samples as when they were in the barrier during operation, but to check if the material retrieved had the same water retention capacity that could be expected for the FEBEX reference bentonite under similar conditions.

7.3. Water retention curve results

The water retention curves obtained for the different samples showed differences even between samples taken from the same block. Although in principle the broad range in the dry densities of the samples, which spanned between 1.39 and 1.58 g/cm^3, could be responsible for these differences −since dry density has an acknowledged effect on the water retention capacity−, no clear relation between dry density and water retention capacity was observed for the samples tested.

However, the initial water content seems to have had a significant influence on the water content evolution during wetting. The initial water content difference between samples was more or less preserved until suction reached values around 10 MPa: samples with higher initial water content kept having higher water contents than the other samples during the wetting path. But when suction decreased below 10 MPa the trend changed. The water contents at the end of the wetting paths were similar for heated and non-heated samples. Besides, the comparison between samples taken at different distances from the heater allows to conclude that the samples submitted to the highest temperatures (above 90°C) had for the lowest suctions the highest water adsorption capacity.

Because the water retention capacity is affected by hysteresis, the particular hydraulic path followed by the samples since the beginning of operation until testing in the laboratory has to be taken into account. The samples from the cool section S59 started their wetting in the barrier from a suction of about 100 MPa (corresponding to hygroscopic conditions), whereas the samples close to the heater started a wetting scanning curve from a much higher suction (400 MPa), because they had experienced previously an intense drying. This could be the reason why the samples from the cool section S59 reached initially higher water contents than the others.

The results presented here obtained in cells have been compared and analysed together with those obtained by measuring in the laboratory the suctions of the blocks (Villar et al. 2017, 2018b). This has allowed to better asses the effect of dry density. For suctions below 20 MPa the samples of lower density had higher water retention capacity, since their porosity was higher. For higher suctions the effect of density was less apparent, but overall the samples tested under different suctions in the desiccators reached lower water contents than those measured in blocks that had the same suctions. The reason probably was the lower dry density of the samples tested in cells with respect to that of the blocks. Experiments performed with the FEBEX bentonite compacted at different dry densities showed that for high suctions the water retention capacity was higher the higher the dry density, although the trend inverted towards lower suctions (Villar 2002).

The comparison of these results with the curve for the reference bentonite compacted to dry density 1.6 g/cm^3 showed that for suctions above 20 MPa the WRCs obtained with sensors were in the range or showed a slightly higher retention capacity than the reference bentonite. In contrast, the WRCs obtained in cells (presented in this report) showed lower retention capacity (lower water contents for the same suction) than the reference bentonite. This can also be explained by the differences in dry density, since the dry densities of the samples tested in cells were mostly below 1.6 g/cm^3 whereas those of the blocks in which suctions higher than 20 MPa were measured were above 1.6 g/cm^3. Despite the scatter of the data, it can be said that the water retention capacity did not noticeably change with respect to the reference bentonite during operation.

Regarding the microstructural changes analysed by MIP occurred during wetting under isochoric conditions, the samples showed two major pore families, as it is customary in the

FEBEX bentonite: a macropore family, with sizes between 15 and 70 µm, and a mesopore family, with sizes between 8 and 15 nm. The results showed that the saturation during the WRC determination resulted in an increase mainly of macropores with respect to the blocks retrieved. However, during operation in the barrier the blocks had experienced a clear increase in the proportion of void ratio corresponding to pores smaller than 50 nm (mesopores and micropores).

To additionally analyse the hydration state from a microstructural point of view, the basal reflection (*d*001 value), which gives an indication of the interlayer distance between smectite particles, was measured by X-ray diffraction. Since the water content of the samples increased during the determination of the WRC, the basal spacings –which depend on the degree of hydration of the interlayer– also increased. The 001 reflection was in fact a double peak for all the samples, what had already been observed for the samples from the blocks. After the WRC determination both the values for the main and for the secondary peaks, but particularly for the secondary one, increased. The values corresponded to a completely developed 2-layer hydrate in transition to a 3-layer hydrate and were coherent with those previously measured in saturated samples of untreated FEBEX bentonite of similar dry density.

7.4. Closure

The water retention curves of samples retrieved from the FEBEX in situ test after 18 years of operation were determined in wetting paths under isochoric conditions with the vapour transfer technique. Samples taken from the driest blocks in the barrier, i.e. those closest to the heater and those from the core of the barrier in cool areas, were used, since the aim of the tests was to check the effect of prolonged and intense drying on the water retention capacity of the bentonite.

The interpretation of the results obtained has to take into account that the retention capacity of the bentonite is affected by temperature, hydraulic history, dry density, stress conditions and salinity, among others. In particular, for the samples tested the initial water content conditioned the retention capacity for suctions above 10 MPa. In contrast, the samples closest to the heater reached higher water contents for the lowest suctions than the rest of the samples, which attest that the water adsorption capacity was not lost as a result of prolonged drying.

The comparison of the WRCs obtained in the retrieved samples with those for the FEBEX reference bentonite compacted at similar densities shows that there were no changes in the water retention capacity during operation and that the water adsorption capacity of the bentonite under constant volume conditions was mostly conditioned by dry density.

Acknowledgements

This work has been financed by the FEBEX-DP consortium (NAGRA, SKB, POSIVA, CIEMAT, KAERI) and through the Annex XLII of the ENRESA-CIEMAT framework agreement. Part of the laboratory work was performed by J. Aroz, R.J. Iglesias, C. Gutiérrez-Álvarez, F.J. Romero and N. Brea.

List of References

AITEMIN 2002. Sensors Data Report (In Situ Experiment). FEBEX Project Deliverable D1-g. Technical Report 70-IMA-L-5-34. Report n. 26 (20.02.97 to 31.07.02) 157 pp.

Bárcena, I, García-Siñeriz, J.L. 2015. FEBEX-DP (GTS) Full Dismantling Sampling Plan (in situ Experiment). Nagra Arbeitsbericht NAB 15-14. 103 pp.

Bárcena, I., Fuentes-Cantillana, J.L., García-Siñeriz, J.L., 2003. Dismantling of the heater 1 at the FEBEX "in situ" test. Description of operations. Publicación Técnica ENRESA 09/2003, Madrid, 134 pp.

Clarke E.C.W., Glew D.N. 1985. Evaluation of the thermodynamic functions for aqueous sodium chloride from equilibrium and calorimetric measurements below 154 °C. J Phys Chem Ref Data 14: 489-610.

ENRESA 1995. Almacenamiento geológico profundo de residuos radiactivos de alta actividad (AGP). Diseños conceptuales genéricos. Publicación Técnica ENRESA 11/95. 105 pp. Madrid.

ENRESA 2000. FEBEX Project. Full-scale engineered barriers experiment for a deep geological repository for high level radioactive waste in crystalline host rock. Final Report. Publicación Técnica ENRESA 1/2000, Madrid, 354 pp.

ENRESA 2006. FEBEX Full-scale Engineered Barriers Experiment, Updated Final Report 1994-2004. Publicación Técnica ENRESA 05-0/2006, Madrid, 590 pp.

Fernández, A.M.,Sánchez-Ledesma, D.M., Melón, A., Robredo, L. M., Rey, J.J., Labajo, M., Clavero, M.A., Carretero, S., González, A.E. 2018. Thermo-hydro-geochemical behaviour of a Spanish bentonite after of the FEBEX in situ test at the Grimsel Test Site.Technical report CIEMAT/DMA/2G216/03/16. NAB16-025. Madrid, 256 pp.

Gmitro, J.I., Vermeulen, T. 1964. Vapor-liquid equilibria for aqueous sulfuric acid. An I. Ch. E. J. 10(5): 740-746.

Iglesias, R.J., Carbonell, B., Villar, M.V. 2018. FEBEX-DP. Postmortem analyses of bentonite performed at CIEMAT. Laboratory sampling logs. Technical Report CIEMAT/DMA/2G218/2/18. Madrid, 116 pp.

Marcial, D. 2003. Comportement hydromécanique et microstructural des matériaux de barrière ouvragée. Ph.D. Thesis. École Nationale des Ponts et Chausées, Paris, 316 pp.

Martínez, V., Abós, H., García-Siñeriz, J.L. 2016. FEBEX-e: Final Sensor Data Report (FEBEX In Situ Experiment). Nagra Arbeitsbericht NAB 16-019. Madrid, 244 pp.

Lide, D.R.(1995): CRC Handbook of Chemistry and Physics. 75th ed. CRC Press.

Lloret, A., Romero, E., Villar, M.V., 2004. FEBEX II Project Final report on thermo-hydro-mechanical laboratory tests. Publicación Técnica ENRESA 10/04, Madrid, 180 pp.

Lloret, A., Villar, M.V. 2007. Advances on the knowledge of the thermo-hydro-mechanical behaviour of heavily compacted FEBEX bentonite. Physics and Chemistry of the Earth Parts A/B/C 32 (8-14): 701-715.

Sánchez, M., 2004. Thermo-hydro-mechanical coupled analysis in low permeability media. PhD Thesis. Universitat Politècnica de Catalunya (UPC), Barcelona, 281 pp.

Savitzky, A., Golay, M.J.E. 1964. Smoothing and differentiation of data by simplified least squares procedures. Analytical Chemistry 36: 1627-1639.

Sing, KSW, Everett, DH, Haul, RAW, Moscou, L, Pierotti, RA, Rouquérol, J & Siemieniewska, T (1985) Reporting physisorption data for gas/solid systems with special reference to the determination of surface area and porosity. Pure & Appl. Chem. 57(4): 603-619. IUPAC.

Villar, M.V. 2002. Thermo-hydro-mechanical characterisation of a bentonite from Cabo de Gata. A study applied to the use of bentonite as sealing material in high level radioactive waste repositories. Publicación Técnica ENRESA 01/2002, Madrid, 258 pp.

Villar, M.V. 2007. Water retention of two natural compacted bentonites. Clays and Clay Minerals 55(3): 311-322.

Villar, M.V. 2017. FEBEX-DP Postmortem THM/THC Analysis Report. NAB 16-017. 143 pp.

Villar, M.V., Lloret, A., 2004. Influence of temperature on the hydro-mechanical behaviour of a compacted bentonite. App. Clay Sci. 26(1-4), 337-350.

Villar, M.V., Gómez-Espina, R. 2009. Report on thermo-hydro-mechanical laboratory tests performed by ciemat on febex bentonite 2004-2008. Informes Técnicos CIEMAT 1178. Madrid, 67 pp. Agosto 2009.

Villar, M.V.; Pelayo, M. & Fernández, A.M. 1996. Sondeos Cortijo de Archidona. Análisis mineralógico y geoquímico preliminar. CIEMAT/IMA/54A40/7/96. Madrid, 26 pp.

Villar, M.V. (Ed.) 2006. FEBEX Project Final report. Post-mortem bentonite analysis. Publicación Técnica ENRESA 05-1/2006, Madrid, 183 pp.

Villar, M.V.; Gómez-Espina, R. & Gutiérrez-Nebot, L. 2012. Basal spacings of compacted bentonite. Applied Clay Science 65-66: 95-105.

Villar, M.V., Iglesias, R.J., Abós, H., Martínez, V., de la Rosa, C., Manchón, M.A. 2016. FEBEX-DP onsite analyses report. NAB 16-012. 106 pp.

Villar, M.V.; Iglesias, R.J.; Gutiérrez, C. & Campos, G. 2017. Use of psychrometers, capacitive sensors and vapour transfer technique to determine the water retention curve of compacted bentonite. In: Ferrari, A. & Laloui, L. (Eds.) Advances in Laboratory Testing and Modelling of Soils and Shales (ATMSS). Springer Series in Geomechanics and Geoengineering, pp 123-130. Springer, Cham, Switzerland. DOI 10.1007/978-3-319-52773-4_13.

Villar, M.V., Iglesias, R.J., García-Siñeriz, J.L. 2018a. A heterogeneous bentonite barrier after 18 years operation. Environmental Geotechnics. https://doi.org/10.1680/jenge.17.00093

Villar, M.V., Iglesias, R.J., Gutiérrez-Álvarez, C., Carbonell, B., Campos, R., Campos, G., Martín, P.L., Castro, B. 2018b. FEBEX-DP: Thermo-hydro-mechanical postmortem analysis of bentonite performed at CIEMAT. Technical report CIEMAT/DMA/2G216/2/16. NAB16-024. Madrid, 144 pp.

1135- 9420